POLITECNICO DI TORINO
Repository ISTITUZIONALE

A control-oriented approach to estimate the injected fuel mass on the basis of the measured in-cylinder pressure in multiple injection diesel engines

Terms of use:

Publisher copyright

(Article begins on next page)

22 September 2024

1   **A CONTROL-ORIENTED APPROACH TO ESTIMATE THE INJECTED FUEL MASS**

2   **ON THE BASIS OF THE MEASURED IN-CYLINDER PRESSURE IN MULTIPLE**

3   **INJECTION DIESEL ENGINES**

4   *Roberto Finesso, Ezio Spessa**

5

6   *IC Engines Advanced Laboratory, Politecnico di Torino*

7   *c.so Duca degli Abruzzi 24, 10129 - Torino, Italy*

8

9   *Key Words: diesel, control-oriented, injection, pilot, main*

10

11   **ABSTRACT**

12   A new control-oriented methodology has been developed to estimate the injected fuel

13   quantities, in real-time, in multiple injection DI diesel engines on the basis of the measured

14   in-cylinder pressure.

15   The method is based on the inversion of a predictive combustion model that was previously

16   developed by the authors, and that is capable of estimating the heat release rate and the in-cylinder

17   pressure on the basis of the injection rate. The model equations have been rewritten in order to

18   derive the injected mass as an output quantity, starting from use of the measured in-cylinder

19   pressure as input.

20   It has been verified that the proposed method is capable of estimating the injected mass of pilot

21   pulses with an uncertainty of the order of ± 0.15 mg/cyc, and the total injected mass with an

22   uncertainty of the order of ± 0.9 mg/cyc. The main sources of uncertainty are related to the

23   estimation of the in-cylinder heat transfer and of the isentropic coefficient $\gamma = c_p/c_v$.

24   The estimation of the actual injected quantities in the combustion chamber can represent a

*Corresponding Author: Tel. +39-011.090.4482; Fax: +39-011.090.4599; e-mail: ezio.spessa@polito.it

powerful means to diagnose the behavior of the injectors during engine operation, and offers

the possibility of monitoring effects, such as injector ageing and injector coking, as well as of

allowing an accurate control of the pilot injected quantities to be obtained; the latter are in fact

usually characterized by a large dispersion, with negative consequences on the combustion

quality and emission formation.

The approach is characterized by a very low computational time, and is therefore suitable

for control-oriented applications.

NOMENCLATURE

A: heat transfer area

AC: Alternating Current

B: Bore diameter

BDC: Bottom Dead Center

BMEP: Brake Mean Effective Pressure

BTDC: Before Top Dead Center

c: coefficient of sensitivity

CA: crank angle

c_0: Woschni heat transfer calibration coefficient

CLD: Chemi-Luminescence Detector

c_P: specific heat at constant pressure

c_v: specific heat at constant volume

DI: Direct Injection

DoE: Design of Experiment

DT: Dwell Time

ECU: Electronic Control Unit

50   *EGR*: Exhaust Gas Recirculation

51   *EOC*: End of Combustion

52   *EOI*: End of Injection

53   *ET*: Energizing Time

54   *EVO*: Exhaust Valve Opening

55   *GMPT-E*: General Motors PowerTrain-Europe

56   *h: heat transfer convective coefficient*

57   H_L: lower heating value of the fuel

58   *HLM*: HRR local minima criterion to estimate the SOC of intermediate pulses

59   *HRR:* Heat Release Rate

60   *ICEAL-PT*: Internal Combustion Engine Advanced Laboratory at the Politecnico di Torino

61   *IMEP*: Indicated Mean Effective Pressure

62   *IVC*: Intake Valve Closing

63   *k*: coverage factor

64   *K*: combustion rate parameter of the heat release model

65   *m*: compression phase polytropic coefficient; mass

66     $\dot{m}_{f,inj}$: fuel injection rate

67   *MFB50:* crank angle at which 50% of the fuel mass fraction has burned

68   *n*: engine speed

69   *NEDC*: New European Driving Cycle

70   *p*: pressure

71   *PCCI:* Premixed Charge Compression Ignition

72   p_f: injection pressure

73   *PFP:* Peak Firing Pressure

74   p_{int}: intake manifold pressure

75   p_m: motored pressure

76   q: generic injected fuel quantity [mm^3]

77    $q_{f,inj}$: total injected fuel quantity [mm^3]

78    $q_{pil,tot}$: total injected fuel quantity of the pilot pulses [mm^3]

79   Q: energy

80   Q_{ch}: released chemical energy

81   Q_{fuel}: chemical energy of the injected fuel

82   Q_{ht}: heat exchanged by the charge with the walls

83    $Q_{ht,glob}$: heat globally exchanged by the charge with the walls over the combustion period

84   Q_{net}: net energy

85   R: gas constant

86   R^2: squared correlation coefficient

87    $RAFR$: relative air-to-fuel ratio

88    $RMSE$: root mean square of the error

89   SOC: Start of Combustion

90   SOI: Start of Injection

91   S_p: Mean piston speed

92   t: time

93   T: temperature

94   TAF: time average filtering

95   T_{int}: intake manifold temperature

96   T_{SOI}: temperature evaluated at SOI

97   T_w: wall temperature

98   TDC: Top Dead Center

4

99   u^2 : variance

100   U: Expanded uncertainty

101   V: volume

102   V_d: cylinder displacement

103   WG: wastegate

104   *Greek Simbols*

105   $\gamma = c_p/c_v$: isentropic coefficient

106   ρ: density

107   ρ_{SOI}: density evaluated at SOI

108   τ: ignition delay parameter of the heat release model

109

110   *Subscripts*

111   *exp*: experimental

112   *f, inj*: injected fuel

113   *f, evap:* evaporated fuel

114   *glob*: global

115   *ht*: heat transfer

116   *inj*: injected

117   *int*: related to the intake manifold

118   *main*: related to the main injection

119   *pil*: related to the pilot injection

120

121   *Superscripts*

122   *SOC*: calculated from the start of combustion

123

126

1. INTRODUCTION

Modern DI diesel engines usually adopt multiple injections in order to optimize pollutant formation, combustion noise and efficiency [1-3]. The injected fuel quantity of each pulse is usually set by the ECU (Electronic Control Unit) in open-loop control mode, on the basis of an injector map; this map usually provides the injected quantity as a function of the energizing time (ET) (i.e., the duration of the electric command provided to the injector) and of the injection pressure (p_f), and is derived from an experimental steady-state characterization of the injectors performed at the hydraulic test bench [4, 5]. However, a real-time control of the actual injected quantities has not yet been developed. The actual quantity of fuel that is injected into the combustion chamber can in fact be very different from that resulting from the steady-state injector map, as a consequence of several effects. First, the dynamic pressure effects that are induced in the pipes by multiple injection strategies may lead to a variability of the actual injected quantities even for a constant ET, depending on the time interval between consecutive injections (i.e., on the dwell-time DT) and on the injection pressure [4, 5]. Moreover, effects such as injector ageing and coking [6] may lead to a worsening of the injection system performance, which cannot currently be predicted by ECUs.

A critical situation occurs for pilot injections, in which the injected quantity is very small. The actual amount of injected fuel mass of the pilot pulses may in fact be highly dispersed during engine operation, and this may depend on the injection parameters (i.e., DT, p_f) or on injection system ageing. Considering that pilot pulses affect pollutant formation [2, 7], and above all soot formation [8] to a great extent, it could be very useful to be able to perform

6

148 real-time diagnostics of the actual injected fuel mass in the combustion chamber during engine

149 operation in order to improve the combustion quality and to reduce engine-out pollutant

150 emissions.

151   Interest in control-oriented predictive combustion models that simulate the heat release rate and

152 in-cylinder pressure in diesel engines has been growing over the last few years, due to their good

153 predictive capability and the increasing computational performance of modern ECUs [9-17]. One of

154 the most widely adopted methods used to simulate the heat release in DI diesel engines is the

155 accumulated fuel mass approach [11-17]. This method is based on the assumption that the rate of

156 released chemical energy is proportional to the energy associated with the fuel quantity made

157 available for combustion at the considered instant. This energy can be computed at time t as the

158 difference between the chemical energy associated with the injected fuel quantity and the

159 cumulative heat release. The accumulated fuel mass method has the great advantage of being able to

160 directly relate the injection rate to the combustion rate, and is therefore physically consistent. This

161 approach has been applied extensively and successfully to a wide range of engine hardware setups

162 and operating conditions [13-17].

163   The capability of this model to correctly correlate the injection rate with the heat release rate has

164 suggested the possibility of using the same model to derive the injected fuel mass as an output

165 quantity, starting from the experimental heat release rate that is obtained from the measured

166 in-cylinder pressure. The model equations have therefore been rewritten in order to derive the

167 injected fuel mass as a function of the heat release rate. The proposed methodology therefore

168 requires the measurement of the in-cylinder pressure, which can be carried out by means of pressure

169 sensors embedded in the glow-plugs (e.g., see [18]); these pressure sensors could also be used for

170 closed-loop combustion control tasks as shown in [18].

171   The investigation has been carried out on a GM 2.0 L diesel engine at several representative

172 key-points of the NEDC (New European Driving Cycle), which feature a pilot-main injection

173   strategy. The approach that is proposed in this study to estimate the actual injected quantities is

174   based on combustion diagnostics; alternative methods based on the measurement of hydraulic

175   variables in the injection system, have already been proposed in the literature, such as those

176   reported in [19-20]. In that study, a miniaturized hot-film anemometer with titanium/platinum

177   metallization was developed on a low-temperature co-fired ceramics substrate and integrated in

178   a Common Rail injection nozzle, so that the injected fluid velocity could be measured. The

179   integration of a ceramic flow sensor chip in the nozzle leads to an additional cost compared to

180   the baseline injector configuration. Moreover, it may cause some disturbances to the fluid

181   properties inside the nozzle and induce a reduction in the injected quantities. However, it offers

182   the advantage of being able to directly monitor the injected fuel velocity in each injector.

183   The method proposed in the present study is based on the measured in-cylinder pressure. This

184   solution also requires an additional cost, related to the need to install integrated pressure sensors

185   in the cylinders; however, these sensors can also be used for additional tasks, such as

186   closed-loop combustion control of combustion phasing. An advantage of the proposed method is

187   that it does not cause disturbances in the fluid properties inside the nozzle; however, a limit in

188   the minimum dwell-time between consecutive injections is introduced, as the method assumes

189   that any heat release overlapping between consecutive injection pulses is negligible.

190   In the present investigation, a comparison was made between the injected quantities that are

191   predicted by the model and those which are derived from the ECU on the basis of the injector

192   map. The total injected quantity predicted by the model was also compared with that derived

193   from a fuel flow meter. The investigation was carried out on some representative operating

194   conditions of the NEDC.

195   A sensitivity analysis on the effects of the main model parameters was also carried out, and

196   the uncertainty of the estimated injected quantities was evaluated.

197   Finally, an analysis of the required computational time was also done.

198

2. TEST ENGINE AND EXPERIMENTAL SETUP

200   The model has been assessed and applied to a Euro 5 GMPT-E 2.0 L engine equipped with a

201 twin-stage turbocharger and with piezo-driven injectors. The main engine specifications are

202 reported in Table 1.

203   **Table 1 – Main specifications of the Euro 5 diesel engine.**

Engine type	2.0L "Twin-Stage" Euro 5
Displacement	1956 cm^3
Bore x stroke	83.0 mm x 90.4 mm
Connecting rod length	145 mm
Compression ratio	16.5
Valves per cylinder	4
Turbocharger	Twin-stage with valve actuators and WG
Fuel injection system	Common Rail 2000 bar piezo
Specific power and torque	71 kW/l – 205 Nm/l
Injector specifications	d=137 μm, C_d = 0.8, C_a =0.84, C_v =0.95

204

205   The experimental data were acquired in a previous research activity that was financially

206 supported by GMPT-E and which had the aim of investigating the potentialities of innovative piezo-

207 and solenoid-driven Common Rail injection systems on engine performance, emissions, fuel

208 consumption and combustion [3]. The experimental tests, related to the engine and to the injectors,

209 were carried out at the highly dynamic test bed and at the hydraulic test rig at ICEAL-PT (Internal

210 Combustion Engine Advanced Laboratory at the Politecnico di Torino).

211   The experimental characterization of the injectors was carried out at the Bosch-Moehwald

212 hydraulic bench [4-5], which is instrumented for a complete fluid-dynamic characterization of

213 Common Rail fuel-injection systems, and includes an EVI injection-rate meter, an EMI2 device to

214 gauge the oil injected mass as well as thermo-piezo-transducers to measure temperature and

215   pressure traces in the rail and at the injector inlet.

216   The engine dynamic test rig was equipped with: an 'ELIN AVL APA 100' cradle-mounted AC

217   dynamometer, featuring a power of 220 kW, a nominal torque of 525 Nm, and a maximum speed of

218   12000 rpm; an 'AVL KMA 4000' system, used to continuously meter engine fuel consumption;

219   an 'AVL AMAi60' raw exhaust-gas analyzer.

220   All of the abovementioned measuring instruments were controlled by the AVL PUMA

221   OPEN 1.3.2 automation system. The test bed environment was interfaced with AVL CAMEO

222   software to run intelligent engine calibration procedures on the basis of the DoE (Design of

223   Experiment) approach.

224   The engine was fully instrumented with piezoresistive pressure transducers and K and T

225   thermocouples to measure the pressure and temperature levels at various engine locations. An

226   'NGK' UEGO air-fuel ratio sensor was placed inside the exhaust system. A Kistler 6058A41

227   high-frequency piezoelectric transducer was fitted to the glow-plug seat to measure the

228   in-cylinder pressure time-histories. The in-chamber pressure traces were referenced on the

229   basis of the pressure in the intake manifold, which was measured by means of a high-frequency

230   Kistler 4075A10 piezoresistive transducer. The latter was located at the inlet runner of the

231   cylinder equipped with the in-cylinder pressure sensor.

232

233   *2.1. Experimental tests*

234   The method was tested on six key-points (expressed in terms of engine speed x BMEP),

235   which were identified in order to characterize the engine operations in a medium-sized

236   passenger car over an NEDC. The key-points are: 1500x2, 1500x5, 2000x2, 2000x5, 2500x8,

237   2750x12 rpm x bar. Table 2 summarizes the main engine parameters for the six analyzed tests.

238   **Table 2 – Main specifications of the six analyzed key-points.**

Key-point	p_f	Intake O_2	p_{int}	q_{pil} (ECU)	$q_{f,inj}$ (ECU)	SOI pil	SOI main
	bar	%	bar	mm³	mm³	deg BTDC	deg BTDC
1500x2	458	15.98	0.963	1.7	7.6	10.7	-2.37
1500x5	589	16.73	1.169	1.6	17.3	12.2	-0.75
2000x2	554	16.58	1.051	1.6	9.3	16.2	-0.86
2000x5	753	16.73	1.373	1.4	18.2	17.0	-0.12
2500x8	1198	17.83	2.01	1.2	33.2	25.4	3.84
2750x12	1481	17.69	2.23	1.1	46.7	30.5	6.63

239

240

241   **3. DESCRIPTION OF THE COMBUSTION MODEL**

242   A detailed description of the model, including the calibration and validation procedures, has

243   already been given in detail in [13-15]. However, a summary is reported hereafter for the sake of

244   clarity.

245   The heat release model is based on the accumulated fuel mass approach, which assumes that, at

246   any time instant, the rate of chemical energy released by the fuel is proportional to the energy

247   associated with the in-cylinder accumulated fuel mass. This energy can be calculated at time instant

248   t as the difference between the chemical energy of the injected fuel mass and the released chemical

249   energy.

250   The released chemical energy $Q_{ch,j}$ at time t, for each pulse j ($1 \leq j \leq N$) of the injection event,

251   is therefore evaluated as follows:

252
$$\frac{dQ_{ch,j}}{dt} = K_j \left[Q_{fuel,j} \left(t - \tau_j \right) - Q_{ch,j} \left(t \right) \right] \qquad (1)$$

253   where K_j and τ_j are model calibration quantities, related to the combustion rate and to the

254   ignition delay, respectively, and $Q_{fuel,j}$ is the chemical energy associated with the injected fuel mass:

255
$$Q_{fuel,j} = \int_{t_{SOI,j}}^{t} \dot{m}_{f,inj} H_L dt \qquad t \leq t_{EOI,j} \qquad (2)$$

256
$$Q_{fuel,j} = \int_{t_{SOI,j}}^{t_{EOI,j}} \dot{m}_{f,inj} H_L dt \qquad t > t_{EOI,j} \qquad (3)$$

11

257   SOI and EOI denote the start and end of injection, respectively, $\dot{m}_{f,inj}$ the injection rate

258   and H_L the lower heating value of the fuel. The total released chemical energy can be calculated

259   as the sum of the contributions of all the injection pulses:

260
$$Q_{ch} = \sum_{j=1}^{N} Q_{ch,j} \qquad (4)$$

261   The K_j and τ_j parameters have to be appropriately tuned in order to obtain a good matching

262   between the predicted Q_{ch} curves and those derived from the experimental in-cylinder pressure

263   [13].

264   The calibration is performed for several steady-state operating conditions, and

265   physically-consistent correlations are then derived as a function of significant engine variables.

266   The tuning procedure of the model for the engine considered in this study is reported in [15].

267   With reference to the combustion rate coefficients, it was found, in [13-15], that a constant

268   value can be taken for the combustion rate parameter of the pilot pulse (i.e., K_{pil}). Instead, it

269   was shown, in [13-15], that a dependence exists between the combustion rate parameter of the

270   main pulse (i.e., K_{main}) and the engine speed/load conditions, and this dependence can be taken

271   into account either by means of a look-up table or by means of simple correlations such as

272   those shown in [13]. In addition, a reduction factor was introduced in [15] to correctly account

273   for low-density/low-oxygen operating conditions, which may induce a remarkable decrease in

274   the combustion rate.

275   The ignition delay parameters were studied in detail in [21], and the following correlations

276   were identified for the engine considered in the present study:

277
$$\tau_{pil} = 0.008977 \rho_{SOI}^2 - 0.36077 \rho_{SOI} + 3.8619 \qquad (5)$$

278
$$\tau_{main} = 3.8E4 \, \rho_{SOI}^{-2.2} \exp^{\left(\frac{2100}{T_{SOI}}\right)} O_2^{-1.9} \, p_f^{-0.31} q_{pil,tot}^{-0.35} \qquad (6)$$

279   Equation (5) indicates that only the charge density calculated at SOI (ρ_{SOI}) is necessary for

280   a good estimation of the ignition delay of the pilot injections, as the physical contribution is

281   predominant over the chemical one [21]. Instead, the effect of the intake charge oxygen

282   concentration (O_2), of the charge density and temperature at SOI (ρ_{SOI}, T_{SOI}), of the injection

283   pressure (p_f) and of the total injected pilot quantity ($q_{pil,tot}$) have to be included to accurately predict

284   the ignition delay of the main pulse.

285   ρ_{SOI} and T_{SOI} are calculated assuming that the in-chamber thermodynamic conditions at BDC

286   are equal to those in the intake manifold (p_{int}, T_{int}):

287
$$\rho_{SOI} = \frac{p_{int}}{RT_{int}} \left(\frac{V_{BDC}}{V_{SOI}} \right) \qquad (7)$$

288
$$T_{SOI} = T_{int} \left(\frac{V_{BDC}}{V_{SOI}} \right)^{m-1} \qquad (8)$$

289   where m is the polytropic coefficient during the compression phase.

290   The choice of using BDC as the reference angle to estimate ρ_{SOI} and T_{SOI} is just a convention.

291   It was in fact verified that the values of ρ_{SOI} and T_{SOI} obtained using, for example, IVC as the

292   reference crank angle are very similar (i.e., the root mean square difference is of the order of 0.34

293   kg/m^3 and 5.3 K, respectively, for the key-points analyzed in the present paper).

294   The values of ρ_{SOI} and T_{SOI} obtained using Eq. (7) and Eq. (8) are obviously approximations of

295   the actual values inside the combustion chamber. The actual values of ρ_{SOI} could be estimated by

296   dividing the total trapped mass by the in-chamber volume at SOI. The total trapped mass is the sum

297   of the trapped air mass, of the trapped EGR mass and of the residual gas mass. The different

298   contributions could be evaluated on the basis of the air-to-fuel ratio and of the EGR rate, which can

299   in turn be estimated with the procedure shown in [22]. The actual T_{SOI} values could instead be

300   evaluated by applying the ideal gas law at SOI, using the values of the in-cylinder pressure at SOI

301   and of the total trapped mass.

302   Figure 1a shows a comparison between the actual values of ρ_{SOI} and those obtained using

303   Eq. (7), while Fig. 1b shows a comparison between the actual values of T_{SOI} and those obtained

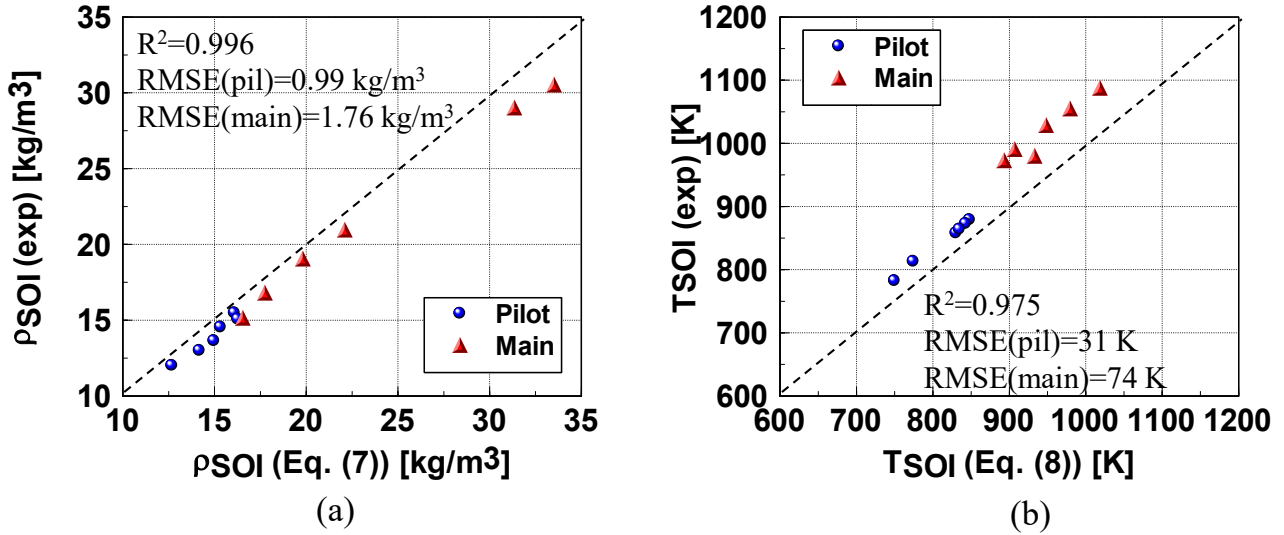304   using Eq. (8), for the key-points analyzed in the present study.

(a)   (b)

305
306   **Figure 1 – Experimental vs. calculated values of ρ_{SOI} using Eq. (7) (a); experimental**

307   **vs. calculated values of T_{SOI} using Eq. (8) (b).**

308   In general, the approximation of the density is quite good, as the average root mean square

309   (RMS) difference is 0.99 kg/m^3 for the $\rho_{SOI,pil}$ term and 1.76 kg/m^3 for the $\rho_{SOI,main}$ term (the

310   use of Eq. (7) leads to an overestimation). With reference to T_{SOI}, it can be seen that the

311   average root mean square difference between the values obtained with Eq. (8) and the actual

312   ones are 31 K for $T_{SOI,pil}$ and 74 K for $T_{SOI,main}$. The underestimation obtained using Eq. (8) is

313   mainly due to the heat transfer effects during the intake phase and to the residual gas

314   contribution being neglected. Moreover, the greater overestimation of $T_{SOI,main}$ is due to the

315   charge heating caused by the pilot combustion being neglected.

316   However, it can be seen, in Fig. 1, that the use of Eqs. (7-8) allows the trends of ρ_{SOI} and

317   T_{SOI} to be captured, so that the differences, with respect to the true values, are indirectly taken

318   into account through the tuning of the exponents in Eqs. (5-6). Moreover, Eqs. (7-8) require the

319   intake manifold pressure and temperature, which are known quantities for the ECU, as input,

320　　and they can therefore be considered suitable for control-oriented applications.

321　　　　O_2 can be derived from the real-time EGR and intake charge model [23], while p_f and

322　　$q_{pil,tot}$ are known quantities for the engine ECU.

323　　　　The predicted released chemical energy Q_{ch} can be used as a starting quantity to evaluate the

324　　charge net energy (i.e., Q_{net}) which is given, at each time instant, by the difference between the

325　　released chemical energy and the heat exchanged by the charge with the walls, i.e., Q_{ht} [24]:

326
$$Q_{net} = Q_{ch} - Q_{ht} \qquad (9)$$

327　　　　Q_{net} can be approximated by means of a uniform scaling of the Q_{ch} curve, according to the

328　　procedure proposed in [13-15]; the scaling factor includes the global heat exchanged between the

329　　charge and the walls over the combustion period, i.e., $Q_{ht,glob}$.

330　　　　The net energy of the charge can therefore be approximated as follows [13]:

331
$$Q_{net}^{SOC} \cong Q_{ch} \frac{m_{f,inj}^* H_L - Q_{ht,glob}}{m_{f,inj}^* H_L} \qquad (10)$$

332　　　　where $m_{f,inj}^*$ is the total injected fuel mass and H_L the lower heating value of the fuel; the

333　　superscript (SOC) indicates that Q_{net} is evaluated from the start of combustion onwards. The $Q_{ht,glob}$

334　　parameter must be known in order to apply Eq. (10). In general, it is necessary to derive a

335　　physically consistent correlation for this parameter, such as that proposed in [13], as a function of

336　　the ratio between the injected fuel quantity and the engine speed. The experimental values of $Q_{ht,glob}$,

337　　which are necessary to identify this correlation, are calculated as the difference between the

338　　chemical energy of the total injected mass (i.e., $m_{f,inj}^* H_L$) and the value of the experimental net

339　　energy curve evaluated at the end of combustion. The experimental net energy curve ($Q_{net,exp}^{SOC}$) can

340　　be derived from the measured in-cylinder pressure using a single zone approach [24]:

341
$$dQ_{net,exp}^{SOC} = \frac{\gamma}{\gamma - 1} p_{exp} dV + \frac{1}{\gamma - 1} V dp_{exp} \qquad (t \geq t_{SOC}) \qquad (11)$$

342 where $\gamma = \dfrac{c_p}{c_v}$ is the ratio of the specific heats, and was evaluated as a function of the

343 relative air-to-fuel ratio, according to the correlation that was proposed in [13]:

344 $$\gamma = -0.0064 RAFR^2 + 0.0563 RAFR + 1.2151 \qquad (12)$$

345 The experimental values of γ used to derive Eq. (12) are shown in Fig. 2, and were derived

346 in [13] for a 1.9L GM diesel engine using different values of the compression ratio. The values of

347 the squared correlation coefficient R^2 and of the root mean square error (RMSE) for the

348 predicted vs. experimental values of γ are also reported in the chart.

$R^2 = 0.93$

$RMSE = 0.006$
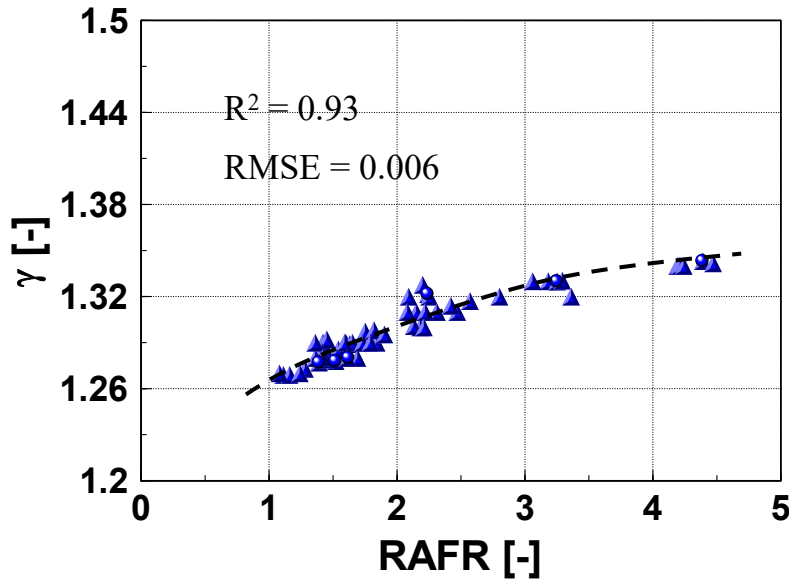
349
350 **Figure 2– Trend of the experimental values of the γ parameter as a function of the**

351 **relative air-to-fuel ratio [13].**

352 The experimental value of $Q_{ht,glob}$ is therefore calculated as follows:

353 $$Q_{ht,glob,exp} = m^*_{f,inj} H_L - Q^{SOC}_{net,exp}(t_{EOC}) \qquad (13)$$

354 It is convenient to use an accurate estimate of the total injected mass in Eq. (13) (e.g., that

355 derived from a fuel flow meter) in order to accurately evaluate the global heat transfer parameter.

356 The calibration of the $Q_{ht,glob}$ parameter was carried out in [13-15] using the values of the fuel

357 flow rate that were measured by means of a fuel flow meter installed at the test bed; this flow rate

358   was split into equal parts over the 4 cylinders, and converted into an average injected mass per cycle.

359   It has in fact been verified that, for the present engine, the performance of the four injectors is similar

360   (see section 3.1).

361   It was found in [13-15] that $Q_{ht,glob}$ is well correlated with the $q_{f,inj}/n$ parameter, where $q_{f,inj}$

362   indicates the total injected quantity of fuel and n the engine speed. The following correlation was

363   derived from engine map tests acquired on a GM 1.9L diesel engine with a similar hardware setup to

364   that of the present study, but equipped with solenoidal injectors (see [14]):

$$Q_{ht,glob} = 7656 \cdot \frac{q_{f,inj}\left[mm^3\right]}{n\left[rpm\right]} + 14.4 \ J \qquad (14)$$

365

366   Figure 3 shows the experimentally-derived values of $Q_{ht,glob}$ that were used to identify Eq. (14)

367   (blue triangles), as well as the experimentally-derived values of $Q_{ht,glob}$ for the six key-points

368   considered in this study (red circles). It can be noted that the values of the key-points are in trend.

369   The values of the squared correlation coefficient R^2 and of the root mean square error (RMSE)

370   for the predicted vs. experimental values of $Q_{ht,glob}$ are also reported in the chart.
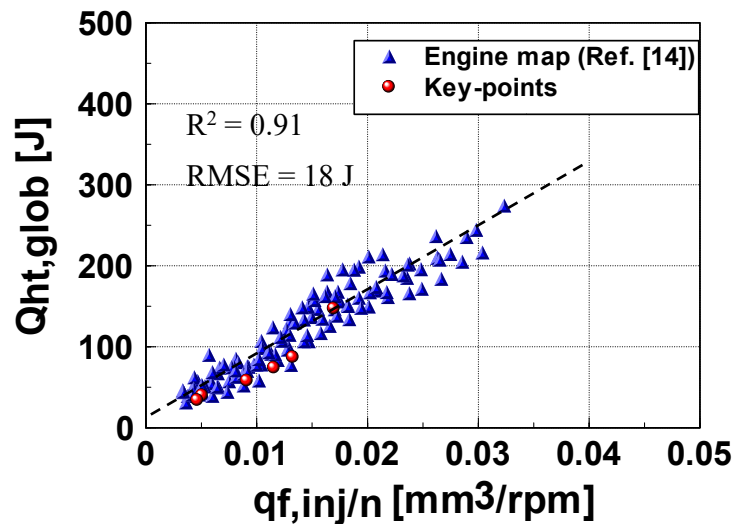
371
372   **Figure 3 – Trend of the experimental values of the $Q_{ht,glob}$ parameter, as a function of the**

373   **qf,inj/n quantity, for the engine map tests of ref [14] and for the key-points of the present**

374   **study.**

17

375

376   It will be shown, in Section 5, that a correct estimation of this parameter is fundamental in order

377   to accurately predict the injected fuel quantities.

378   The estimation of the net energy of the charge, i.e., Q_{net}, allows the in-cylinder pressure to

379   be predicted in the interval between SOC and EOC, using a single zone approach, as follows:

380
$$dp = \left(\frac{\gamma - 1}{V} \right) \left(dQ_{net} - \frac{\gamma}{\gamma - 1} pdV \right) \quad (15)$$

381   The reconstruction of the complete in-cylinder pressure trace also includes the

382   compression and expansion phases, which are modeled by means of polytropic evolutions, and

383   the gas exchange phases, which are modeled as constant pressure evolutions (see [13-15]). In

384   particular, the following correlations were used to estimate the polytropic coefficients of the

385   compression and expansion phases:

386
$$m = 0.0011 q_{f,inj}(mm^3) + 1.30 \quad (16)$$

387
$$m' = -0.0016 q_{f,inj}(mm^3) + 1.38 \quad (17)$$

388

389   *3.1 Analysis of the cylinder-to-cylinder dispersion of the injectors*

390   Although only a single cylinder was instrumented for the pressure measurements, the

391   cylinder-to-cylinder dispersion of the injectors installed on the present engine was verified

392   indirectly on the basis of the analysis of the measured gas temperatures in the four exhaust

393   runners. In general, the temperatures of the exhaust gases outflowing from each cylinder depend

394   on combustion phasing (related to the injection phasing), on the air-to-fuel ratio (related to the

395   injected fuel quantity) and on heat transfer effects in the cylinders and in the runners. Outer

396   cylinders are in general characterized by higher heat transfer rates than inner ones.

397   Figure 4 reports the values of the exhaust gas temperatures in the four runners (Fig. 4a), as

398 well as the differences between the temperatures of the cyl1-cyl4 and cyl2-cyl3 exhaust runners (Fig.

399 4b).

400 It can be noted that the outer cylinders are characterized by systematically lower temperatures

401 than the inner ones, due to a higher heat transfer rate. However, by comparing the temperatures of the

402 outer cylinders (cyl1, cyl4), as well as those of the inner cylinders (cyl2, cyl3), it can be noted that the
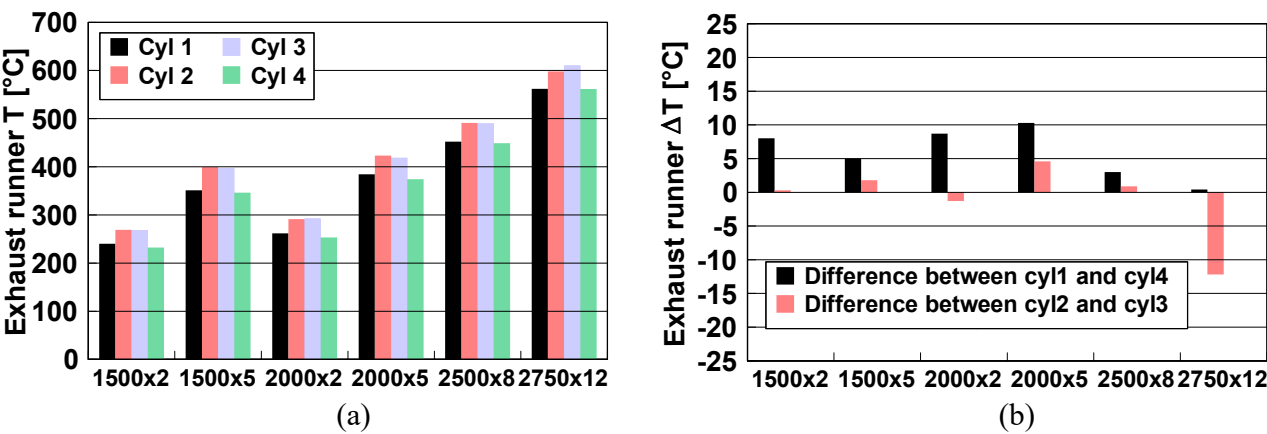
403 differences are small (i.e., of the order of 5-10°C)

(a)   (b)

404
405 **Figure 4 – Values of the gas temperatures in the exhaust runners of the four cylinders (a);**

406 **differences between the temperatures of the gases in the cyl1 and cyl4 exhaust runners, as well**

407 **as between the cyl2 and cyl3 ones (b).**

408

409 This indirectly confirms that the behavior of the injectors installed in cyl1 and cyl4, as well as of

410 those installed in cyl2 and cyl3, is very similar in terms of injection phasing and total injected

411 quantity. In order to verify this, the combustion model was applied to the six key-points to test the

412 impact of a deviation of ±2 deg in the injection phasing of the main pulse, as well as of a deviation ±1

413 mg in the injected quantity, on the predicted in-cylinder temperatures at EVO. The results are shown

414 in Tab. 3.

415

416 **Table 3 – Impact of variations in SOI$_{main}$ and in the injected fuel mass on T$_{EVO}$, using the**
417 **combustion model**

Key-point	SOI$_{main}$+2deg	SOI$_{main}$-2deg	m$_{f,inj}$+1mg	m$_{f,inj}$-1mg
	ΔT_{EVO} [°C]	ΔT_{EVO} [°C]	ΔT_{EVO} [°C]	ΔT_{EVO} [°C]
1500x2	-4.6	5.3	36.8	-37.5
1500x5	-7.7	8.6	26.9	-27.0
2000x2	-6.0	6.5	37.0	-37.8
2000x5	-8.6	9.2	25.5	-26.2
2500x8	-10.5	11.3	18.1	-18.2
2750x12	-13.6	14.5	15.5	-15.6

It can be noted that the experimental differences in the exhaust gas temperatures shown in Fig. 4b correspond to a lower dispersion of the injected quantities than 1 mg/cyc for the same SOI$_{main}$, or to a lower dispersion of SOI$_{main}$ than 2 deg for the same m$_{f,inj}$.

Moreover, in a recent research activity devoted to the refinement of the combustion model [17], each cylinder of a 1.6L GM engine has been instrumented with pressure transducers. It has been verified that the average cylinder-to-cylinder dispersion of IMEP was of the order of 0.6 bar (corresponding to a dispersion of the total injected quantity of about 0.5 mg/cyc), and that the average cylinder-to-cylinder dispersion of MFB50 was of the order of 0.5 deg. This confirms that the injector dispersion in modern diesel engines is very low.

4. ESTIMATION OF THE INJECTED MASS ON THE BASIS OF THE MEASURED IN-CYLINDER PRESSURE

The combustion model inversion procedure, which allows the injected fuel mass to be calculated as a model output, starting from the measured in-cylinder pressure time-histories, is reported hereafter.

A pilot-main injection strategy has been considered for the development of the method, which is however of general application. It has been assumed that the dwell-time between consecutive injections is not too short, so as to prevent overlapping of the heat release contributions that stem from the different injection pulses.

438   The dwell time threshold generally depends on the specific engine operating condition. In order

439   to give some general indications, a dwell-time sweep was simulated using the combustion model for

440   the six key-points. A threshold was identified for each key-point, under which a significant

441   overlapping of heat release occurs between the pilot and main pulses. The thresholds are reported in

442   Tab. 4.

443   **Table 4 – Estimated dwell-time threshold necessary to avoid significant overlapping between**
444   **the pilot and main heat release**

	DT Threshold [μs]
1500x2	300
1500x5	400
2000x2	500
2000x5	500
2500x8	600
2750x12	600

445

446   Starting from Eq. (1), the $Q_{fuel}(t-\tau_j)$ term is made explicit as a function of $Q_{ch,j}$ for each injection

447   pulse j, as follows:

$$Q_{fuel,j}\left(t-\tau_j\right) = Q_{ch,j}\left(t\right) + \frac{1}{K_j}\frac{dQ_{ch,j}}{dt}(t) \quad (18)$$

449   It is therefore necessary to obtain an experimental estimation of the $Q_{ch,j}$ curve for each

450   injection pulse in order to evaluate the $Q_{fuel}(t-\tau_j)$ term. The estimation can be made as follows.

451   First, Eq. (11) is applied to evaluate the whole trend of the experimental charge net energy (i.e.,

452    $Q_{net,exp}^{SOC}$) on the basis of the measured in-cylinder pressure.

453   The calculation is performed from SOC to EOC (a conventional EOC angle, e.g., 430°, can be

454   assumed). The estimation of SOC is therefore necessary; this can be done according to the procedure

455   illustrated in [21].

456   Once the estimation of $Q_{net,exp}^{SOC}$ has been carried out, the experimental trend of the released

21

457   chemical energy (i.e., $Q_{ch,exp}^{SOC}$) is drawn by scaling the $Q_{net,exp}^{SOC}$ curve as follows:

458

$$Q_{ch,exp}^{SOC} \cong Q_{net,exp}^{SOC} \frac{Q_{net,exp}^{SOC}(t_{EOC}) + Q_{ht,glob}}{Q_{net,exp}^{SOC}(t_{EOC})} \qquad (19)$$

459   This is the inverse procedure to that used to estimate the Q_{net} curve on the basis of the Q_{ch}

460   curve predicted by the combustion model (see Eq. (10)). The $Q_{ht,glob}$ parameter was introduced

461   in Eq. (10) and represents the heat globally exchanged between the charge and the walls during

462   combustion; it can be evaluated through Eq. (14), which was derived from experimental tests.

463   As an example, Fig. 5 reports, for the 1500x5 key-point, the experimental Q_{net} curve

464   (dotted red line) and the experimental Q_{ch} curve obtained with Eq. (19) (black line). The $Q_{ht,glob}$

465   parameter is also indicated in the figure. In addition, the experimental Q_{ch} curve obtained using

466   a detailed heat transfer model is also reported with a blue chain line.

467
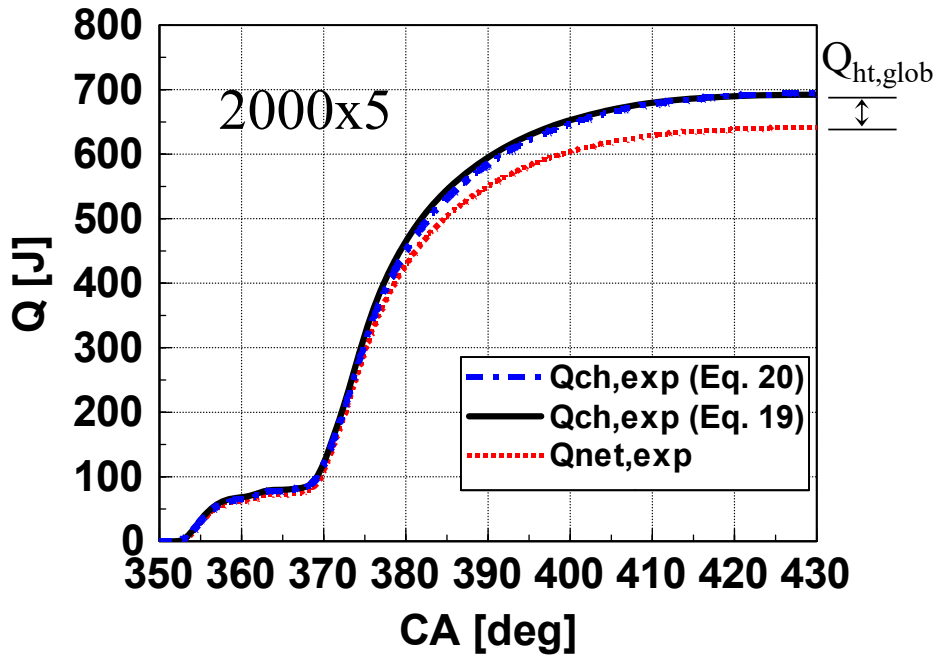
468
469   **Figure 5 – Trends of the experimental net and chemical energy release for the 2000x5**

470   **key-point. The chemical energy release curves obtained from Eq. (19) and using a**

471   **detailed heat transfer model (Eq. (20)) are reported.**

22

472

The detailed heat transfer model is based on a convective formula [25]:

$$\dot{Q}_{ht} = hA(T - T_w) \quad (20)$$

where h is the convective heat transfer coefficient, A is the instantaneous heat transfer area, T is the instantaneous gas temperature and T_w is the wall temperature.

The convective heat transfer coefficient h [W/m²K] was modeled using the Woschni correlation [26]:

$$h[W/m^2K] = c_0 B[m]^{-0.2} p[bar]^{0.8} T[K]^{-0.53} w[m/s]^{0.8} \quad (21)$$

$$w = \left[c_1 S_p[m/s] + c_2 \frac{V_d[m^3] T_r(IVC)}{p_r(IVC) V_r[m^3](IVC)} (p - p_m) \right] \quad (22)$$

where B is the bore diameter, S_p is the mean piston speed, V_d is the cylinder displacement, while T_r, p_r and V_r represent the in-cylinder temperature, pressure and volume at the moment of intake valve closure, respectively. c_0 was used as a calibration factor, while c_1 and c_2 were kept constant and equal to nominal values of 0.0039 and 2.31, respectively.

It can be observed, in Fig. 5, that the simplified procedure used to estimate Q_{ch} (i.e., Eq. (19)) leads to a good approximation of that obtained with the detailed heat transfer model (i.e., using Eq. (20)), even though a slight overestimation occurs for intermediate CA values between SOC and EOC. Similar trends were obtained for the other key-points, but the results are not reported here for the sake of brevity.

The approach based on the detailed heat transfer model requires the estimation of the instantaneous in-cylinder temperature, which is evaluated through the ideal gas law, using the measured in-cylinder pressure and the total trapped mass in the cylinder as input data. The latter quantity includes the contributions of air, EGR and residual gas.

This approach requires a higher computational time effort than the simplified approach (i.e., Eq.

495   (19)), and computational time is a critical parameter for control-oriented applications.

496   Once the $Q_{ch,exp}^{SOC}$ curve has been evaluated, it is necessary to split this curve into the single

497   contributions that stem from each injection pulse. As previously stated, it is assumed that

498   consecutive injections are scheduled using a moderately long dwell-time, in order to reduce the

499   overlapping of the heat release contributions that stem from the different pulses.

500   First, it is necessary to identify the SOC of each injection pulse. This can be done by

501   means of the methods reported in [21]. The overall SOC (i.e., that of the most advanced

502   injection pulse) is evaluated as the crank angle at which the first chemical energy fraction is

503   released. The SOC of the subsequent injection shots is detected by identifying the relative

504   minima of the HRR curve. This procedure is referred to as the "HRR local minima" (HLM)

505   method.

506   At this point, the experimental chemical energy release of the different injection pulses j

507   (i.e., $Q_{ch,j,exp}$, where j ranges from 1 to N, 1 indicates the most advanced pulse and N indicates

508   the most delayed one) can be calculated as follows. With reference to the most advanced pulse

509   (i.e., j=1):

510
$$
\begin{aligned}
Q_{ch,1,exp} &= Q_{ch,exp}^{SOC} \quad (t_{SOC} \leq t < t_{SOC,2}) \\
Q_{ch,1,exp} &= Q_{ch,exp}^{SOC}(t_{SOC,2}) \quad (t \geq t_{SOC,2})
\end{aligned}
\tag{23}
$$

511   where SOC is the overall start of combustion and SOC,2 is the SOC of the second

512   injection pulse.

513   The contribution of the chemical energy release of the subsequent pulses, excluding the

514   last one (i.e., 2≤j≤N-1), is instead calculated as follows:

515
$$
\begin{aligned}
Q_{ch,j,exp} &= Q_{ch,exp}^{SOC} - Q_{ch,exp}^{SOC}(t_{SOC,j}) \quad (t_{SOC,j} \leq t < t_{SOC,j+1}) \\
Q_{ch,j,exp} &= Q_{ch,exp}^{SOC}(t_{SOC,j+1}) - Q_{ch,exp}^{SOC}(t_{SOC,j}) \quad (t \geq t_{SOC,j+1})
\end{aligned}
\tag{24}
$$

516   Finally, the contribution of the chemical energy release of the most delayed pulse (i.e.,

24

517   j=N), is derived as follows:

$$Q_{ch,N,exp} = Q_{ch,exp}^{SOC} - Q_{ch,exp}^{SOC}(t_{SOC,N}) \qquad (t_{SOC,N} \leq t \leq t_{EOC}) \qquad (25)$$

519   The procedure is illustrated in Fig. 6 for the 2000x5 key-point featuring a pilot-main injection

520   strategy.
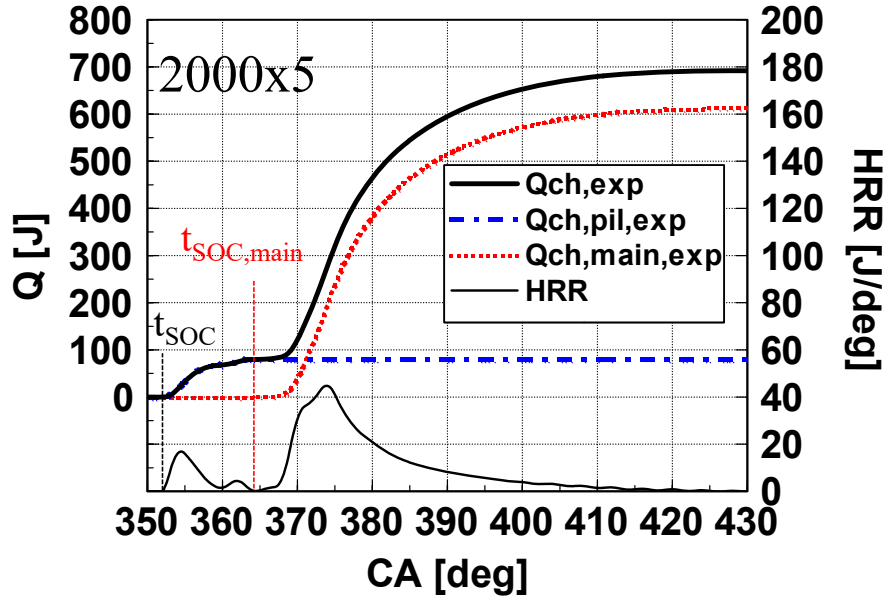
Figure 6 – Trends of the global experimental chemical energy release and contributions of the pilot and main injections evaluated with Eqs. (23-25) for the 2000x5 key-point. The trend of HRR is also reported.

526   Figure 6 reports the overall experimental chemical energy curve (thick black line), as well as

527   the contributions of the pilot (blue chain line) and main (pointed red line) pulses evaluated by

528   means of Eqs. (23-25). The SOC instants evaluated with the above-mentioned procedures are also

529   indicated, as is the HRR curve (thin black line).

530   The $Q_{fuel,j}$ term can now be estimated at time t through the following equation, which is derived

531   from Eq. (18) taking the τ_j parameter into account:

$$Q_{fuel,j}(t) = Q_{ch,j}(t+\tau_j) + \frac{1}{K_j}\frac{dQ_{ch,j}}{dt}(t+\tau_j) \qquad (26)$$

533   The τ_j parameters are estimated by means of Equations (5-6); when input variables related

534   to the injected quantities are used in the correlations to evaluate the model parameters (i.e., τ_j),

535   the values derived from the injector maps can be used, to avoid iterative procedures; it was in

536   fact verified that the resulting error in the evaluation of the ignition delay parameters is

537   negligible.

538   The injected fuel mass curve of each injection pulse j can be estimated as follows:

539
$$m_{f,inj,j} = \frac{Q_{fuel,j}}{H_L} \qquad (27)$$

540   Finally, the total injected quantity of each pulse can be estimated evaluating the

541   steady-state final value of the injected mass curve evaluated by means of Eq. (27).

542   The overall injected fuel mass curve, i.e., $m_{f,inj}$, is obtained by summing the contributions

543   of all the injection pulses:

544
$$m_{f,inj} = \sum_{j=1}^{N} m_{f,inj,j} \qquad (28)$$

545   Figure 7 shows a scheme that summarizes the proposed methodology.
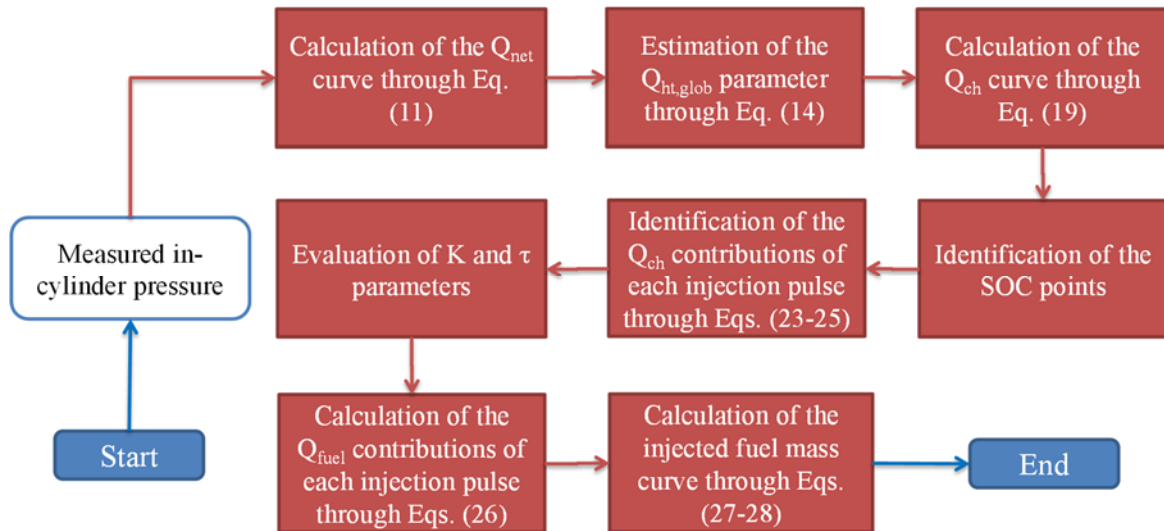
Figure 7 – Scheme of the proposed methodology.

548 **5. RESULTS AND DISCUSSION**

549   The procedure explained in Section 4 was applied to the six key-points whose

550 specifications are reported in Tab. 2. In particular, a comparison was made between the injected

551 fuel mass estimated by means of the proposed method and those derived from the injector map;

552 moreover, a sensitivity analysis was carried out on the main model parameters, and the uncertainty

553 of the pressure-derived values of the injected fuel mass was evaluated.
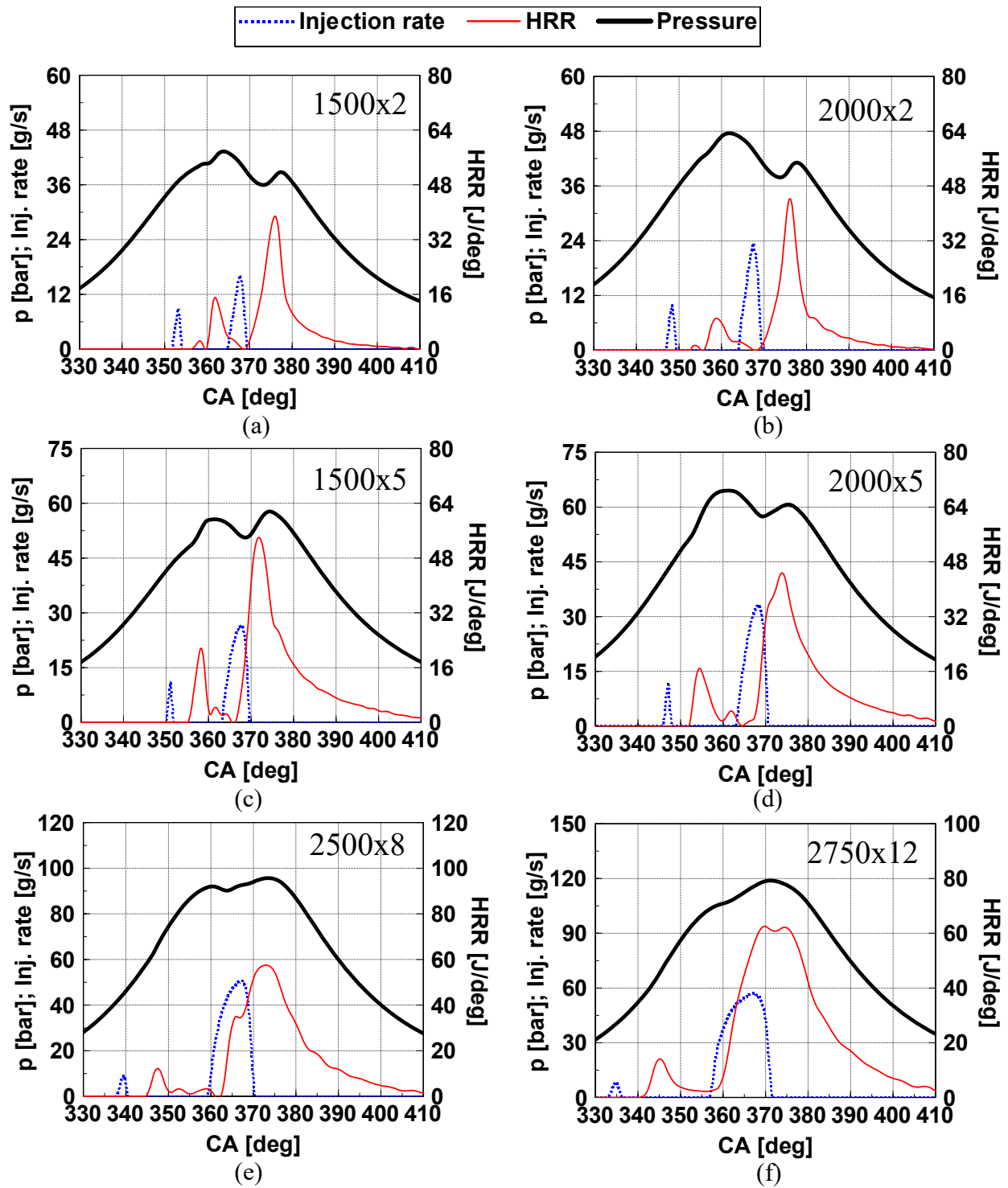
Figure 8 – Trends of the measured in-cylinder pressure, of the pressure-derived HRR and of the injection rate, for the six key-points.

Figure 8 reports the measured in-cylinder pressure trends (black lines), the HRR curves derived from the pressure traces using a single-zone model (thin red lines) and the injection

559 rate profiles (pointed blue lines) for the six key-points. The in-cylinder pressure traces shown in Fig.

560 8 were obtained as the average of 100 consecutive cycles, which were filtered using the TAF

561 (Time-average filtering) procedure shown in [27]. This procedure is based on the following steps.

562 First, the time average of the instantaneous pressure is evaluated in the discrete consecutive CA

563 intervals into which the engine cycle is divided, and the resulting averaged pressure values, taken in

564 the middle of the respective intervals, are interpolated through cubic spline fitting to obtain the

565 original in-cylinder pressure curve.

566   It can be noted, in Fig. 8, that all the key-points feature a pilot-main injection strategy.

567 Moreover, it can be observed, from the HRR traces, that the 1500x2, 2000x2 and 1500x5 key-points

568 show dominant premixed combustion, while the remaining key-points show a premixed-mixing

569 controlled combustion type. It can be noted that HRR premixed and mixing controlled combustion

570 peaks for the latter key-points are of the same order of magnitude, due to the adoption of a pilot

571 injection which leads to a reduction in the premixed combustion contribution. A single injection

572 strategy would lead to much higher HRR peaks during the premixed combustion phase.

573   With reference to the model outcomes, Figure 9a reports, for the six key-points, the values of

574 the pressure-derived total injected fuel mass, as well as the values obtained from the injector map

575 and those derived from the fuel flow meter, while Fig. 9b reports the differences between the values

576 obtained from the injector map/fuel meter and those derived from the measured pressure. Figure 9c,

577 instead, reports the values of the pressure-derived pilot injected quantities as well as those derived

578 from the injector map, while Fig. 9d shows the differences between the values obtained from the

579 injector map and those derived from the measured in-cylinder pressure. Figures 6b-d also report the

580 average uncertainty bands of the proposed method. The procedure to estimate the uncertainty is

581 explained in Section 5.2.

(a) – Pilot+main
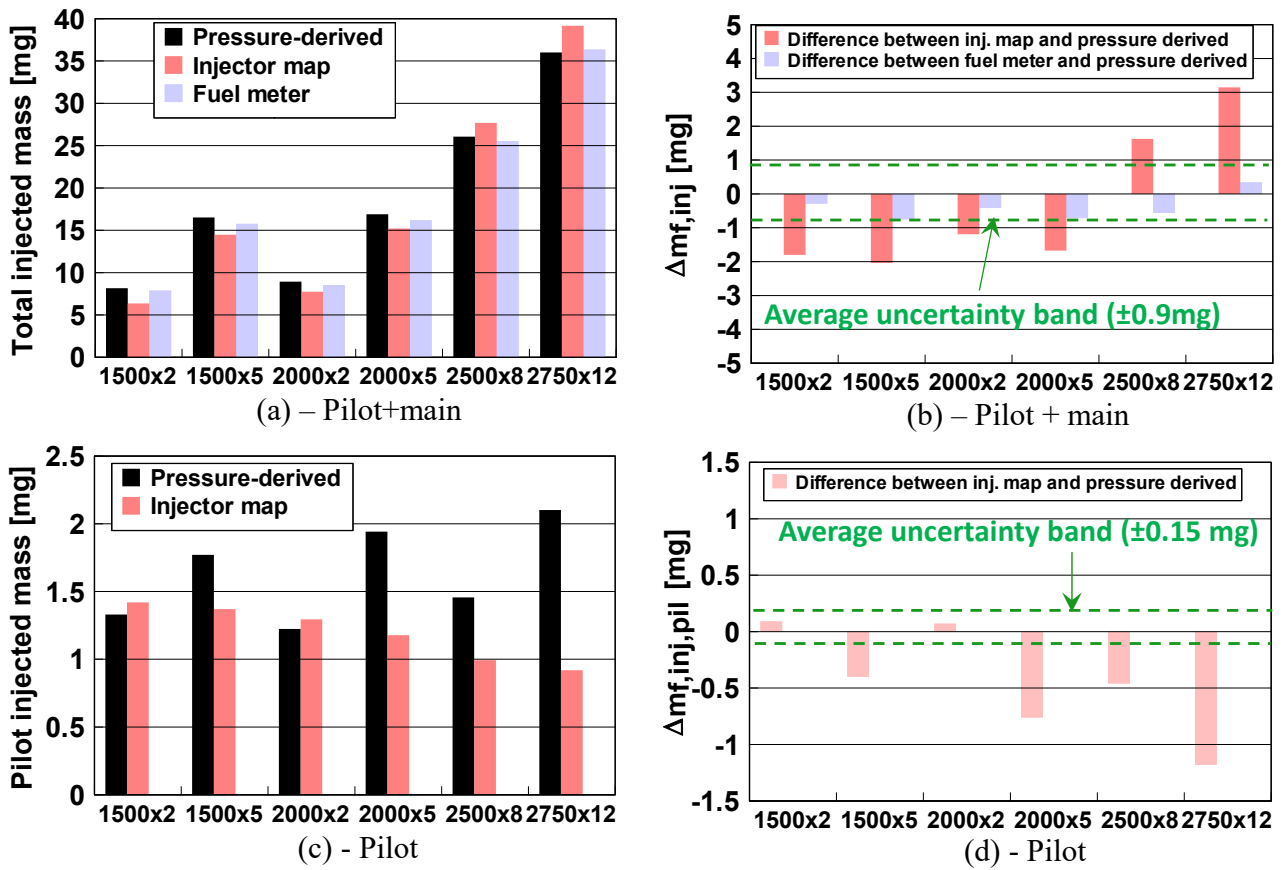
(b) – Pilot + main

(c) - Pilot

(d) - Pilot

Figure 9 – Comparison between the total (a) and pilot (c) fuel injected quantities derived from the in-cylinder pressure and those derived from the injector map (total, pilot) and fuel meter (total); difference between the injected quantities from the injector maps/fuel meter and those obtained from the in-cylinder pressure (b, d). The average uncertainty bands in the estimation of the pressure-derived injected quantities are also reported.

First, it can be noted that the average uncertainty in the evaluation of the injected mass of the pilot pulses is very small (Fig. 9d), as it is of the order of 0.15 mg. The average uncertainty in the evaluation of the total injected quantity is instead of the order of 0.9 mg, and it will be shown, in Section 5.2, that this value mainly depends on the uncertainty in the evaluation of the heat transfer parameter ($Q_{ht,glob}$) when Eq. (14) is used.

596

597   From the results reported in Fig. 9a-b, it can be observed that the pressure-derived total

598   injected quantities are comparable with those derived from the fuel meter, as the difference is below

599   the uncertainty band of the method. It can also be noted that the proposed method diagnoses several

600   deviations in the total injected quantities estimated by the injector map, (i.e., by the ECU): the

601   quantities of the medium-low load key-points (i.e., 1500x2-5, 2000x2-5) are underestimated, while

602   those of the medium-high load key-points (i.e., 2500x8, 2750x12) are overestimated. In particular,

603   the deviations of the ECU-derived total injected quantities are of the order of +3 mg for the

604   2750x12 key-point, of +1.7 mg for the 2500x8 key-point, of -1.5 mg for the 1500x2 and 2000x5

605   key-points and of -2 mg for the 2000x5 key-point. These deviations can be considered significant,

606   compared with the uncertainty of the method.

607   With reference to the pilot injected quantities, it can be observed that the method diagnoses

608   significant deviations in the quantities evaluated by means of the injector map at the 2750x12

609   key-point (-1.3 mg), at the 2000x5 (-0.8 mg) key-point, but also at the 1500x5 and 2500x8

610   operating conditions (about -0.4/-0.5 mg).

611

612   5.1 *Sensitivity analysis*

613   A sensitivity analysis was carried out in order to verify the effect of the main model parameters

614   on the pressure-derived injected quantities. The first three parameters that were considered in this

615   analysis are the values of the K_j coefficients of the combustion model (see Eq. (26)), the value of

616   the isentropic coefficient γ used in Eq. (11) to derive the experimental Q_{net} trace from the

617   in-cylinder pressure and the $Q_{ht,glob}$ parameter used in Eq. (19) to obtain the experimental Q_{ch} trace,

618   starting from the experimental Q_{net} trace; finally, the effect of horizontal and vertical shifts in the

619   in-cylinder pressure trace were also investigated.

620   Each parameter was varied separately, keeping the remaining ones unchanged. The analysis

621　was made for the all the key-points. Reasonable variation ranges were chosen for the

622　parameters considered in the sensitivity analysis.

623
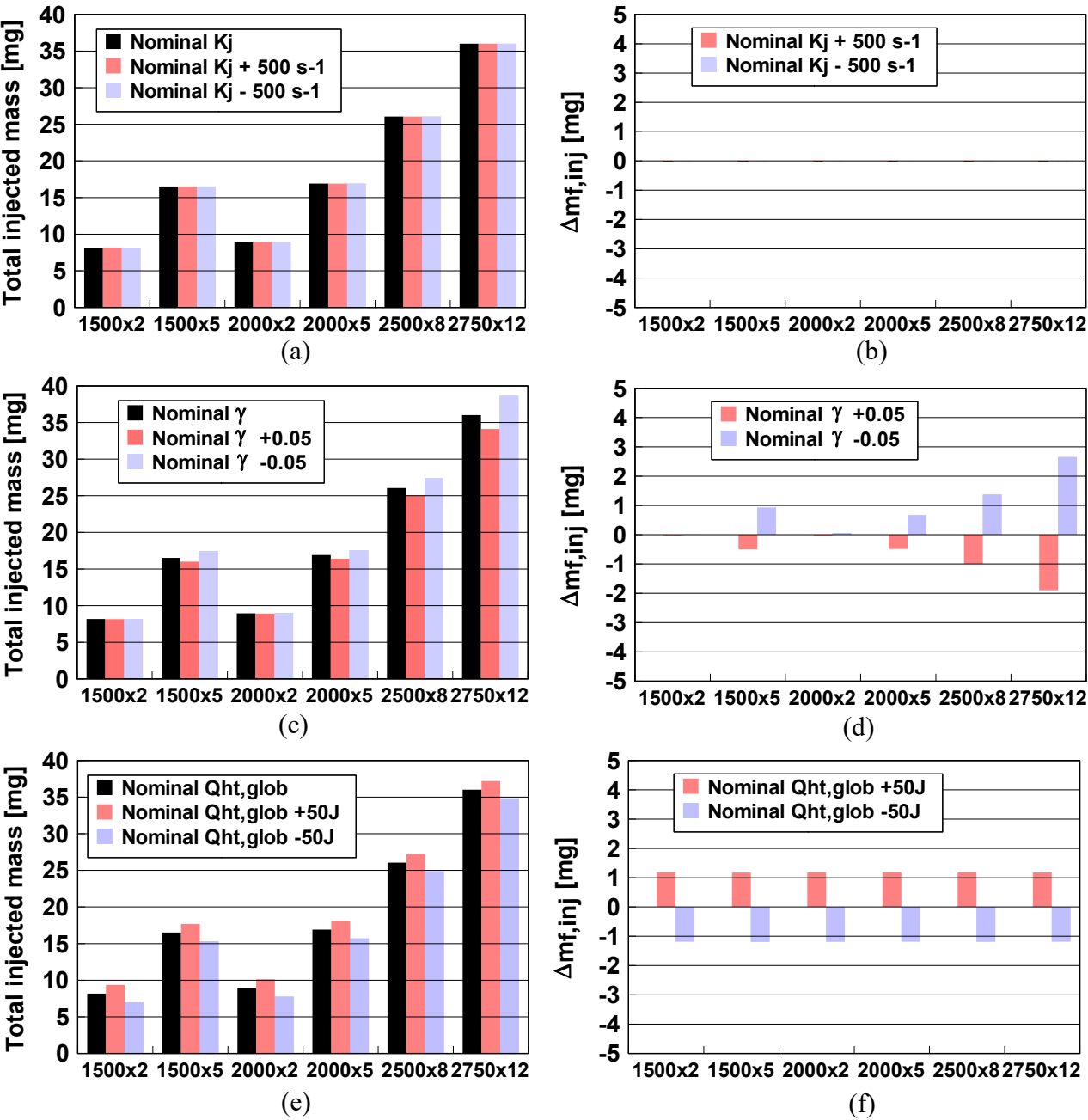
624
625　**Figure 10 – Effect of a variation in the values of the K_j, γ and $Q_{ht,glob}$ parameters**

626　**(with respect to the nominal values) on the estimated total injected mass (a, c, e). The**

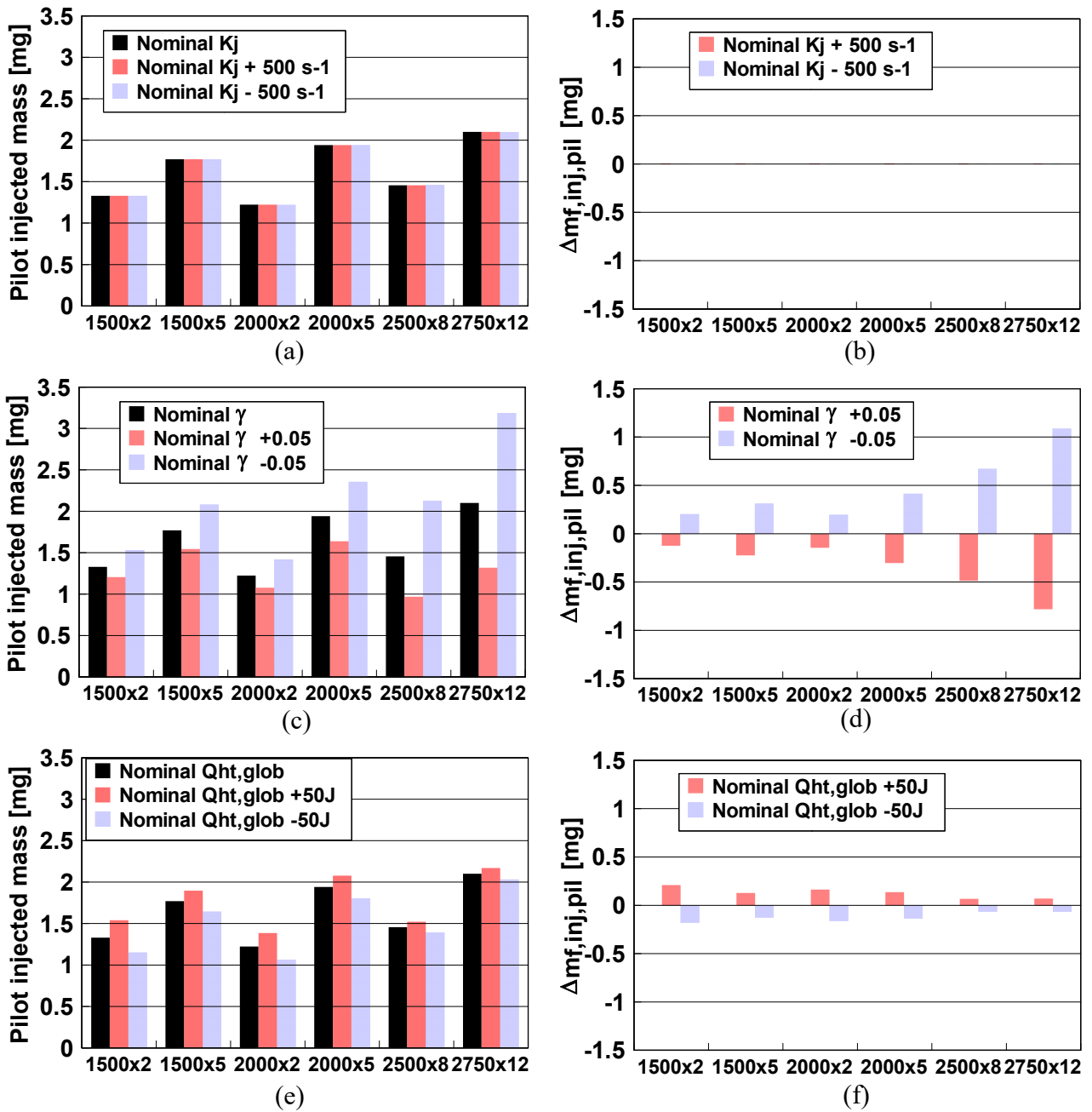627　**differences are also reported (b, d, f).**

628

Figure 11 – Effect of a variation in the values of the K_j, γ and $Q_{ht,glob}$ parameters (with respect to the nominal values) on the estimated pilot injected mass (a, c, e). The differences are also reported (b, d, f).

The results are shown in Figs. 10-13. Figures 10-11 report the effect of a variation in the values of the K_j (Figs. 10a, 11a), γ (Figs. 10c, 11c) and $Q_{ht,glob}$ (Figs. 10e, 11e) parameters, with respect to the nominal values, on the estimated total injected quantities (Fig. 10) and pilot injected quantities

637   (Fig. 11). The differences are also reported in Figs. 10b, 10d, 10f and 11b, 11d,11f.

638   It can be noted that a variation in the values of the K_j parameter (Figs. 10a,b and 11a,b)

639   does not influence the pressure derived injected quantities to any great extent; a variation in the

640   values of the γ parameter has a remarkable effect on both the pressure-derived total injected

641   quantity (Figs. 10c, d) and on pilot injected quantity (Figs. 11c, d), and the effect increases with

642   the engine load. Finally, it is interesting to note that a variation in the value of $Q_{ht,glob}$ mainly

643   affects the diagnosed total injected quantities (the deviations are independent of the engine

644   load/speed), but has little influence on the diagnosed pilot injected quantities.

645   This analysis suggests that is important to accurately select the γ parameter to evaluate the

646   charge net energy Q_{net} (see Eq. (11)), as it can significantly affect the estimation of the total and

647   pilot injected quantities. Moreover, a good prediction of the heat transfer parameter $Q_{ht,glob}$ is

648   also required, as it directly affects the estimated total injected quantity. However, the impact of

649   this parameter on the estimated values of the pilot injected quantities can be considered

650   negligible, and this leads to low uncertainty, as will be shown in Section 5.2.

651   The estimation of the injected quantities could also be affected by an error in the measured

652   in-cylinder pressure trace, which is the main model input. Figures 12-13 report the effect of

653   horizontal and vertical shifts in the in-cylinder pressure trace on the estimated total injected

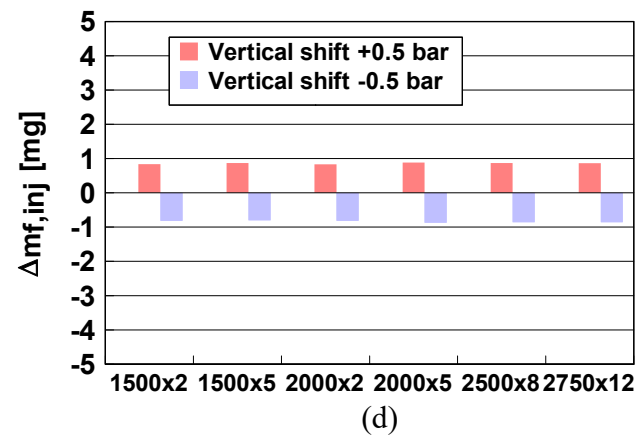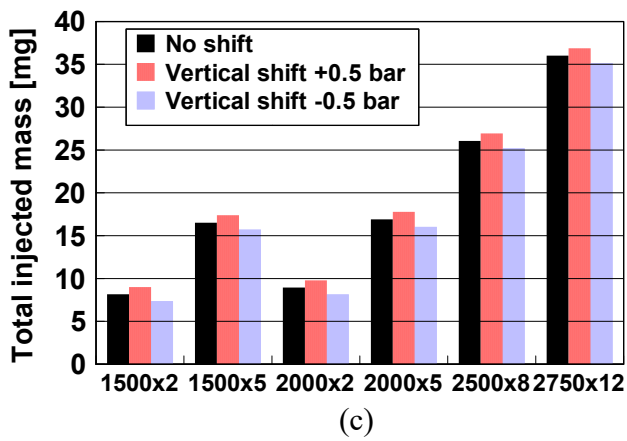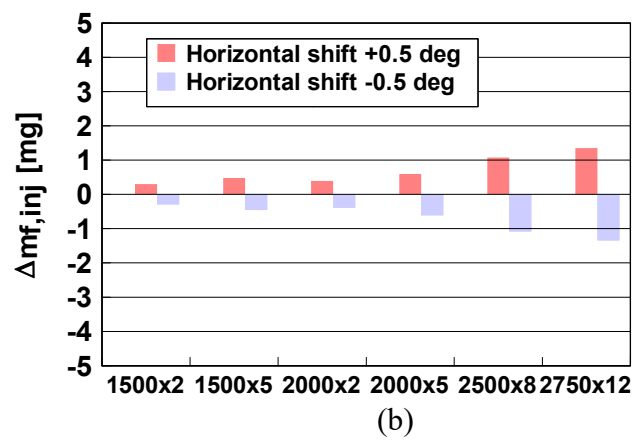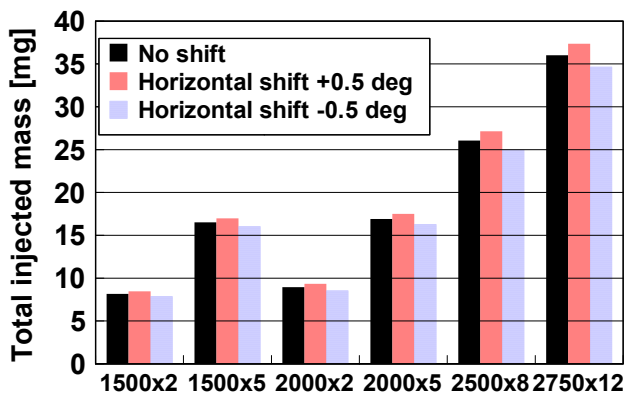654   quantities (Fig. 12) and pilot injected quantities (Fig. 13).

Figure 12 – Effect of a horizontal and vertical shift of the measured pressure on the estimated total injected mass (a, c). The differences are also reported (b, d).
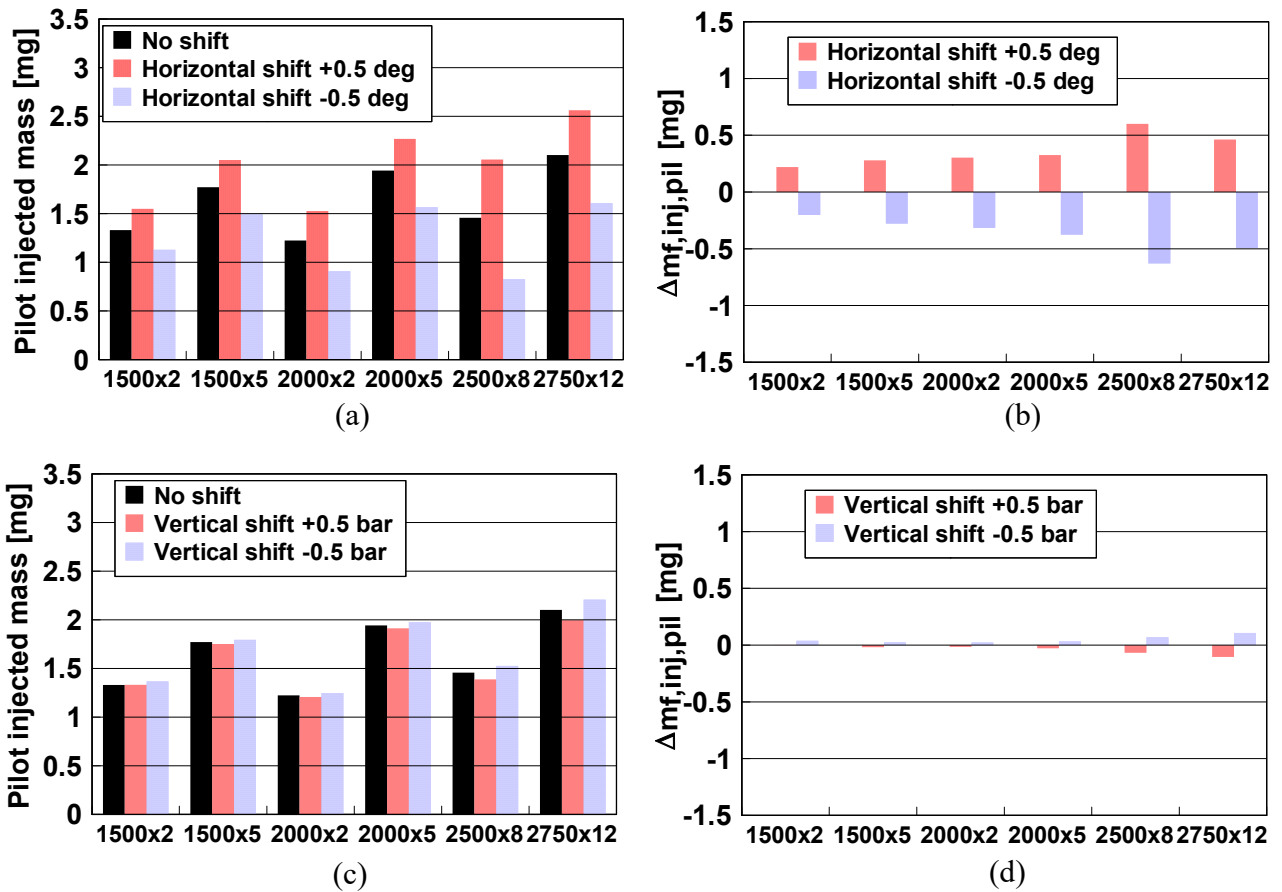
Figure 13 – Effect of a horizontal and vertical shift of the measured pressure on the estimated total injected mass (a, c). The differences are also reported (b, d).

It can be observed, in Fig. 12, that both horizontal and vertical shifts affect the pressure-derived total injected quantities to a great extent, and that the effect of a horizontal shift increases with engine load, while that of a vertical shift is somewhat constant.

With reference to the estimated pilot injected quantities (Fig. 13), it should be noted that a horizontal shift leads to significant deviations, which increase with the engine load, while a vertical shift has little influence.

As a result, attention should be paid to the correct pressure phasing, with respect to the crank angle, and to the correct in-cylinder pressure referencing. The latter may be realized comparing the values of the in-cylinder pressure around BDC with the values measured in the

672   intake manifold by means of an absolute pressure transducer.

673

674   5.2 *Evaluation of the experimental uncertainty*

675   The procedure applied for the evaluation of experimental uncertainties is based on the

676   recommended practices reported in [28] and hereafter summarized.

677   Given an output quantity y, which is dependent on N independent x_i variables, the associated

678   variance $u_c^2(y)$ is calculated through the following relation:

679
$$u_c^2(y) = \sum_{i=1}^{N} \left(\frac{\partial y}{\partial x_i} \right)^2 u^2(x_i) = \sum_{i=1}^{N} c_i^2 u^2(x_i) \quad (29)$$

680   Equation (29) is consistent if the mutual effects between independent variables are neglected. c_i

681   is the "coefficient of sensitivity" of the output quantity y with respect to the *i-th* independent

682   variable x_i.

683   Once $u_c^2(y)$ has been evaluated, it is possible, by assuming a level of confidence (e.g., 95%)

684   and a correspondent coverage factor k (e.g., equal to 2), to evaluate the expanded combined

685   uncertainty of y, $U_c(y)$:

686
$$U_c(y) = k\sqrt{u_c^2(y)} \quad (30)$$

687   If the independent variables x_i are the result of a measurement, the associated variance should

688   be estimated by taking into account the accuracy of the instrument declared in the calibration

689   certificate, the repeatability, the instrument resolution and the master uncertainty.

690   The procedure was used to estimate the uncertainty in the predicted values of the injected pilot

691   mass and of the total injected quantity for the six analyzed key-points.

692   The main parameters that could affect the estimation of the injected quantities were identified

693   and analyzed in Section 5.1. However, most of those parameters can be excluded from the

694   uncertainty calculation as they are not sources of error. First, it was shown that the K_j parameters

695   used in the heat release model do not affect the predicted injected quantities to any great extent

696   (see Fig. 10a, 11a). The γ coefficient has remarkable influence on the predicted quantities (see

697   Fig. 10b, 11b), and it should therefore be selected accurately. The correlation developed in [13],

698   as a function of the RAFR parameter, was used in the present study (see Fig. 2 and Eq. (12)).

699   The $Q_{ht,glob}$ parameter also has a significant effect on the estimated total injected quantities (see

700   Fig. 10c) but has little influence on the estimated pilot injected quantities (see Fig. 11c).

701   Vertical and horizontal shifts in the in-cylinder pressure affect the estimation of Q_{net} and

702   therefore of the pressure-derived injected quantities (see Fig. 11-12). However, if the

703   in-cylinder pressure is referenced correctly (using, for example, an absolute pressure sensor in

704   the intake manifold) and phased correctly (on the basis of the thermodynamic loss angle, see

705   [29]), this error contribution can be excluded from the uncertainty calculation procedure.

706   The only parameters whose effect on the uncertainty of the method has been considered

707   significant are therefore γ and $Q_{ht,glob}$. These parameters were evaluated, in this study, by means

708   of the correlations expressed in Eq. (12) and Eq. (14), and shown in Fig 2 and Fig. 3,

709   respectively. There are two main sources of error for each of the two parameters; the first one is

710   related to the uncertainty in the input variables that are used in the correlations (i.e., RAFR in

711   Eq. (12), $q_{f,inj}$ and n in Eq. (14)). The second source of error is related to the dispersion of the

712   predicted values of γ and $Q_{ht,glob}$ (through Eq.(12) and Eq. (14), respectively) with respect to

713   the experimental ones; this dispersion was quantified by means of the RMSE parameter, which

714   is equal to 0.006 for the γ parameter and to 18 J for the $Q_{ht,glob}$ parameter, using the proposed

715   correlations. The first source of error was evaluated for each parameter (γ, $Q_{ht,glob}$) by applying

716   Eq. (29) to the analytical expression of γ and $Q_{ht,glob}$ expressed by Eqs. (12, 14), and assuming

717   reasonable values for the variance of the RAFR, $q_{f,inj}$ and n parameters. The second source of

718   error was evaluated on the basis of the RMSE values. However, it has been verified that the

719 first source of error is two orders of magnitude lower than the second one. Moreover, it has also

720 been verified that the contribution of γ is low, compared to that of $Q_{ht,glob}$, but it increases with the

721 engine load (as can also be seen in Figs. 10d, 11d).

722 Table 5 summarizes the expanded combined uncertainty of the pressure-derived pilot and total

723 injected quantities. It can be noted that the uncertainty in the evaluation of the pilot quantity is very

724 small, as its average is of the order of 0.15 mg. The average uncertainty in the evaluation of the total

725 quantity is instead of the order of 0.9 mg, and is larger at higher engine loads. This uncertainty is

726 mainly related to the dispersion of the predicted values of $Q_{ht,glob}$ by means of Eq. (14), and could be

727 reduced if a more refined method were to be identified to estimate heat transfer.

728

729 **Table 5 – Evaluation of the expanded uncertainty U of the predicted injected quantities.**

Key-point	Pilot	Pilot+main
	mg	mg
1500x2	0.15	0.85
1500x5	0.10	0.87
2000x2	0.15	0.85
2000x5	0.12	0.86
2500x8	0.15	0.90
2750x12	0.24	1.02

730

731 5.3 *Analysis of the cycle-by-cycle variations and considerations on the in-cylinder pressure quality*

732 The proposed methodology has also been tested on single, independent cycles in order to verify

733 its capability of estimating cycle-by-cycle variations in the injected quantities. Moreover, the same

734 analysis has been carried out using the acquired raw pressure, without TAF filtering, in order to

735 verify the effect of signal noise on the outputs. This is an important aspect, as the use of the

736 proposed method in commercial engines would require integrated pressure sensors, which are

737 characterized by a higher signal noise than the Kistler sensor used in the present investigation.

738   Figures 14-15 report the estimated total and pilot injected quantities, respectively, for 10

739   consecutive cycles using both filtered and raw pressure, for the six key-points.

(a) – 1500x2

(b) – 1500x5

(c) – 2000x2
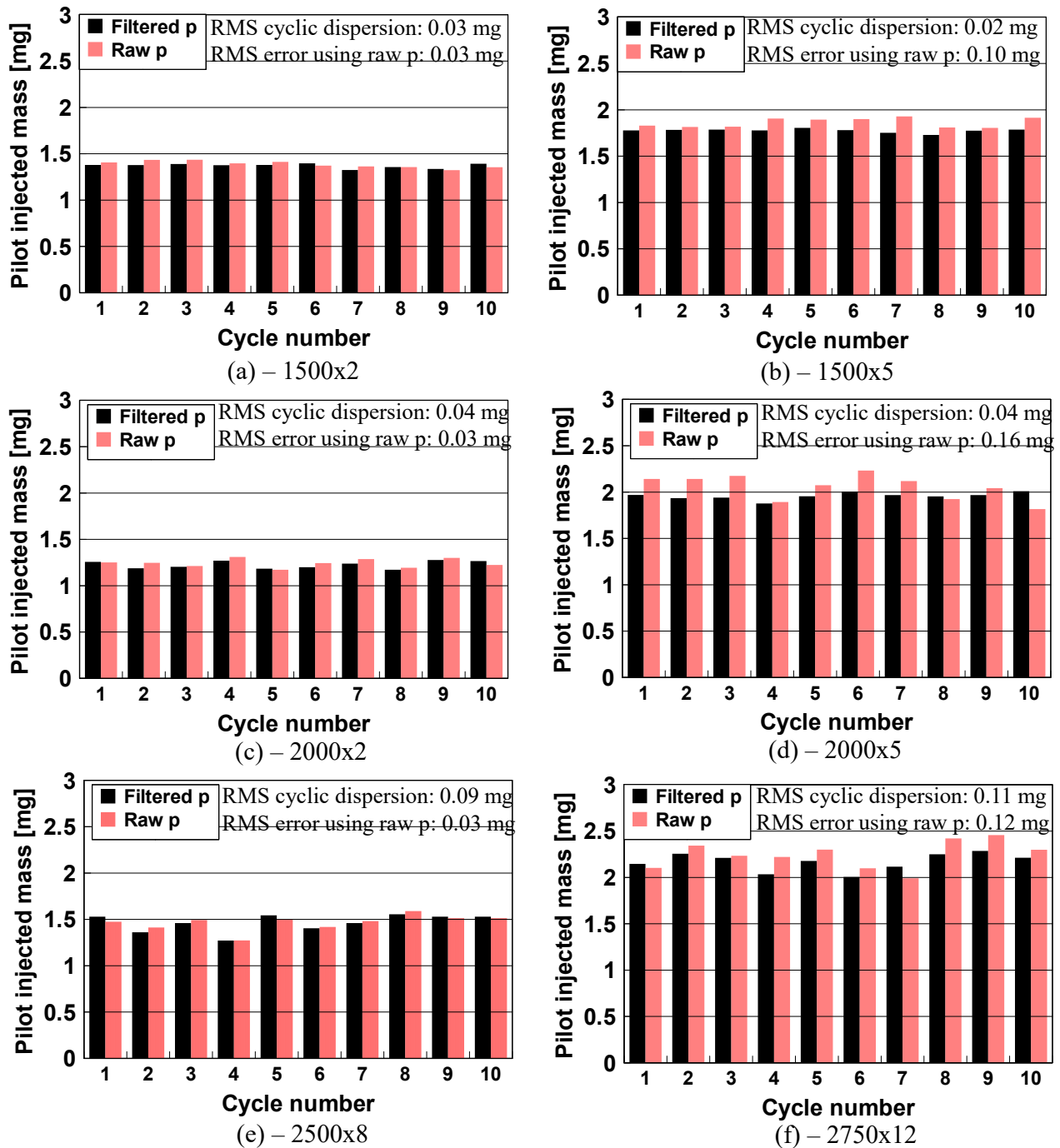
(d) – 2000x5

(e) – 2500x8

(f) – 2750x12
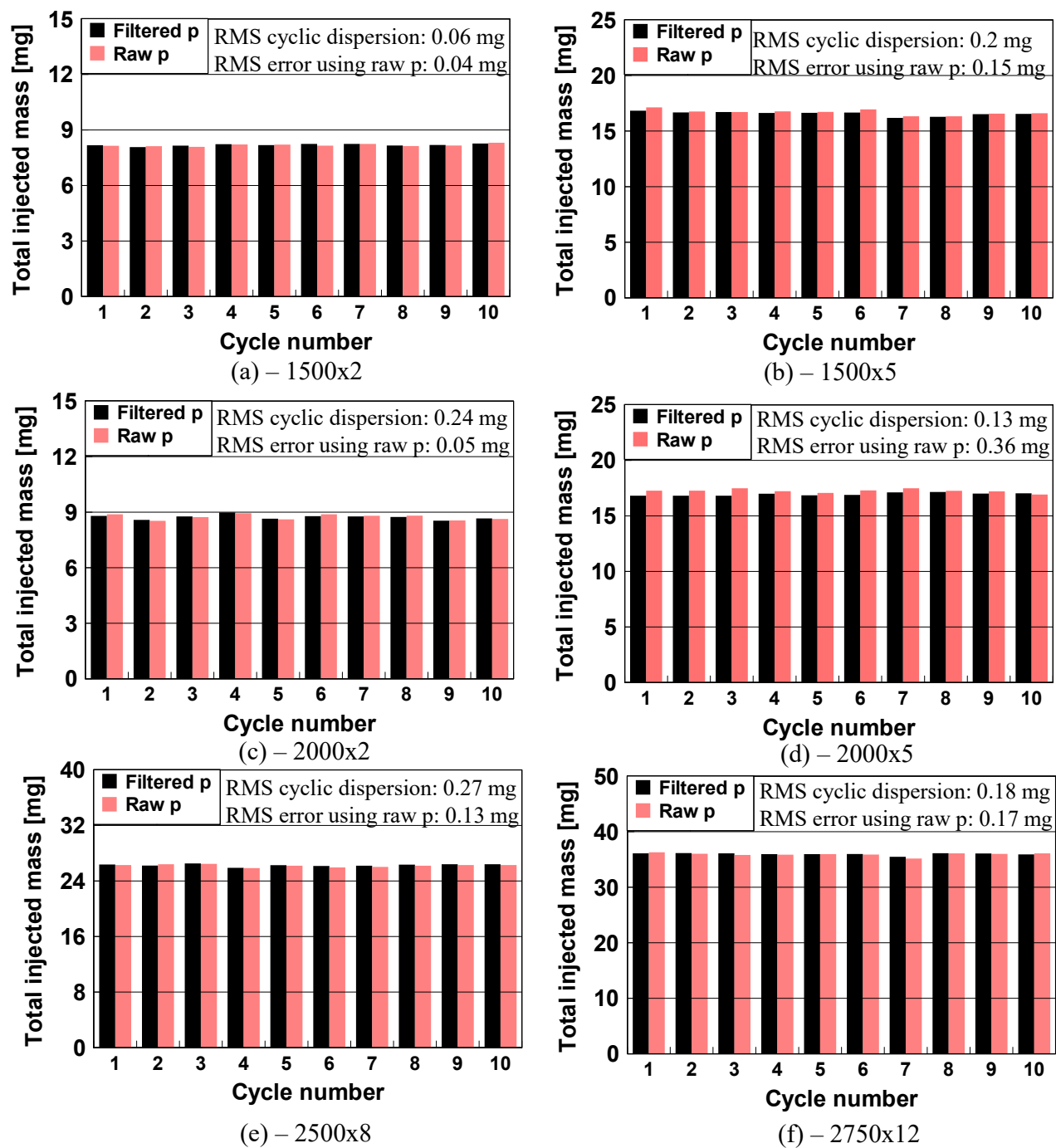
740

741   **Figure 14 – Estimated total injected quantity for 10 consecutive cycles using both**

742   **filtered and raw pressure. The RMS cyclic dispersion (calculated using the filtered**

743   **pressure) and the RMS error of the raw pressure-derived quantities with respect to those**

744 **derived from the filtered p are also reported.**

745

(a) – 1500x2

(b) – 1500x5

(c) – 2000x2

(d) – 2000x5

(e) – 2500x8

(f) – 2750x12

746
747 **Figure 15– Estimated pilot injected quantity for 10 consecutive cycles using both filtered**

748 **and raw pressure traces. The RMS cyclic dispersion (calculated using the filtered pressure)**

749 **and the RMS error of the raw pressure-derived quantities with respect to those derived from**

the filtered pressure are also reported.

The RMS cyclic dispersion (calculated using the filtered pressure) and the RMS error of the injected quantities obtained from the raw pressure, with respect to those derived from the filtered pressure, are also reported in the graphs.

It can be noted that, in general, the cycle-by-cycle dispersion of both the pilot and total injected quantities is very low.

The method is also robust with respect to the use of a raw in-cylinder pressure signal. In this case, the errors depend on the specific engine operating conditions. The largest RMS errors occur at the 2750x12 and 2000x5 key-points, and are of the order of 0.36 and 0.17 mg/cyc, respectively, for the main pulse (see Fig. 14) and of the order of 0.12 and 0.16 mg/cycle, respectively, for the pilot pulses (see Fig. 15).

The use of a raw in-cylinder pressure is therefore suitable for estimating average injected quantities for all the operating conditions, while an accurate evaluation of cycle-by-cycle dispersion in general requires filtering of the pressure trace.

5.4 *Analysis of the computational time*

The computational time is basically expected to depend on the crank-angle step used for the in-cylinder pressure; this step should be chosen on the basis of a trade-off between the calculation time and the prediction accuracy.

An analysis has therefore been carried out in order to evaluate the impact of the crank-angle step on the computational time and on the prediction accuracy of the injected fuel quantities.

The elaboration was performed with the Labwindows CVI software, using a Pentium-D

42

774   PC.

775   The effect of the crank-angle step on the average computational time necessary to run a

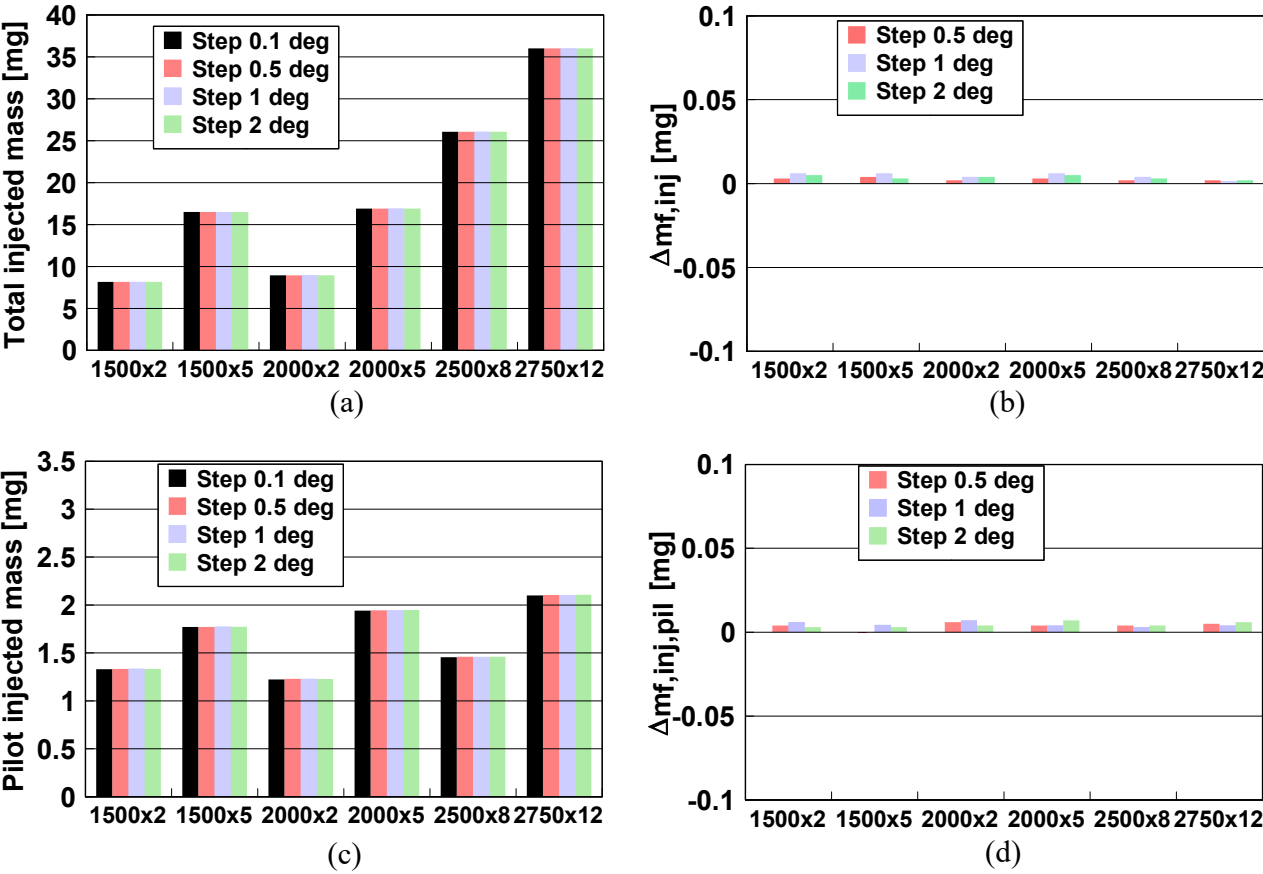776   single operating condition is reported in Tab. 6.

777

778   **Table 6 – Effect of the crank angle step on the computational time.**

Calculation step [deg]	0.1	0.5	1.0	2
Computational time: [ms]	3.4	0.9	0.6	0.3

779

780   Figure 16, instead, shows the effect of the crank angle step used for integration on the

781   estimated total and pilot injected quantities.

782
783   **Figure 16 – Effect of the crank angle step used for integration on the estimated total and**

784   **pilot injected quantities. The differences with respect to the case at 0.1 deg are also reported**

(b, d).

The analysis shows that the procedure is very robust with respect to the crank angle step used for integration. It should be specified that the net energy of the charge was calculated according to Eq. (11), using the trapezoidal rule for integration; it has been verified that this integration rule provides a nearly-independent trend of the net energy with respect to the crank angle step used for integration. The computational time that is required for a crank angle step of 2 deg is of the order of 0.3 ms. Therefore, the method can be considered suitable for control-oriented applications.

6. FUTURE WORK

In addition to the injected quantities, the proposed methodology also has the potential of estimating the injection rate curve on the basis of the measured in-cylinder pressure. This can be done by deriving Eq. (28) with respect to time.

An example is reported in Fig. 17 for the 1500x5 and 2000x5 key-points.

In particular, Fig. 17 reports a comparison between the injection rate profiles obtained with the measured in-cylinder pressure (black lines) and the experimental ones (dotted red lines).
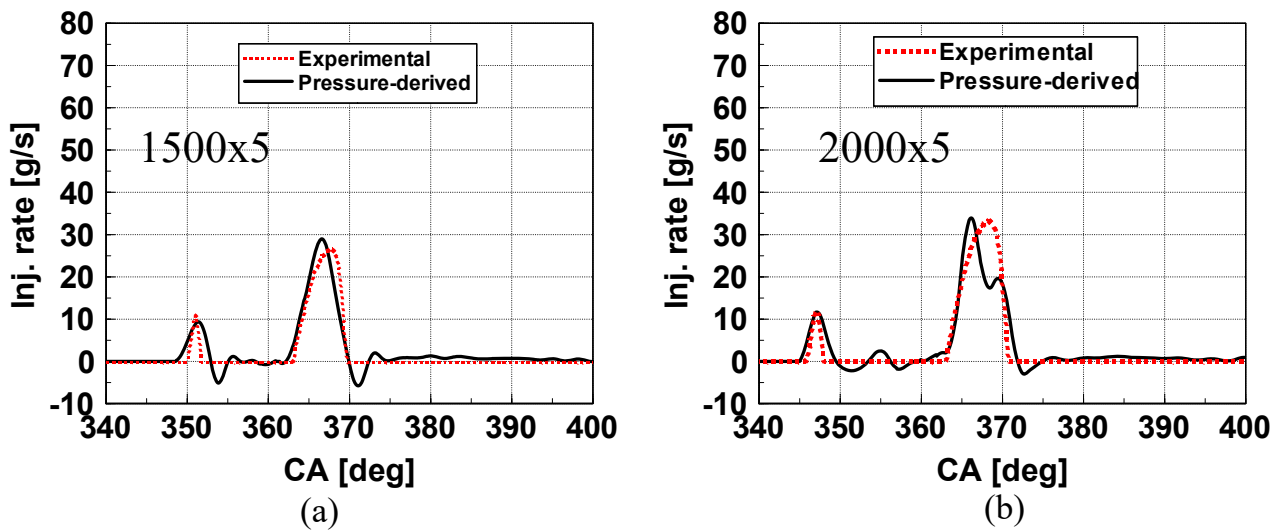
Figure 17 – Comparison between the pressure-derived injection rate profiles and the experimental ones for the 1500x5 and 2000x5 key-points.

It should be noted that the evaluation of the shape of the injection rate is quite good for the 1500x5 key-point, while it shows a double-peak characteristic for the main injection of the 2000x5 key-point. The accuracy of the prediction of the injection rate depends exclusively on the capability of the heat release model to correctly reproduce the HRR shape on the basis of the injection rate profile. It can therefore be observed, in Fig. 17, that the accumulated fuel mass approach (i.e., Eq. (1)) provides good results if the HRR shape is mainly of the premixed type, but is less accurate if the HRR shape is of the premixed-mixing controlled type (see Fig. 8). The result is that the injection rate shape derived from the in-cylinder pressure reflects the premixed-mixing controlled characteristics of the HRR (see Fig. 17b). A refinement in the prediction of the injection rate shape could be realized by refining the heat release model, using, for example, a crank-angle dependent value of the K_j parameters of Eq. (1). This investigation is currently ongoing.

Moreover, the applicability of the proposed method to highly premixed combustion modes, such as PCCI (Premixed Charge Compression Ignition) should also be verified.

45

7. CONCLUSION

A new methodology has been developed to estimate injected fuel quantities on the basis of the measured in-cylinder pressure in multiple injection DI diesel engines.

The method is based on the inversion of a predictive combustion model that was previously developed by the authors, and which is based on the accumulated fuel mass approach.

A sensitivity analysis has been carried out in order to verify the effects of variations in the main input parameters on the calculated injected quantities. It has been found that errors in the estimation of the global heat transfer of ± 50J can lead to errors in the estimation of the total injected quantities of about 1 mg/cyc, but the effect on the estimated pilot quantity error is much smaller (below 0.2 mg/cyc). Moreover, errors in the estimation of the isentropic coefficient γ of ± 0.05 lead to large errors for both the estimated total injected quantity (of up to 2 mg/cyc) and for the estimated pilot quantity (of up to 1 mg/cycle). It has also been verified that horizontal shift errors on the in-cylinder pressure of ± 0.5 deg lead to errors in the estimated total and pilot quantities of up to 1 mg/cyc and 0.5 mg/cyc, respectively, and vertical shift errors on the in-cylinder pressure of ± 0.5 bar lead to errors in the estimated total quantity of up to 0.8 mg/cyc, while the impact on the pilot quantity estimation error is negligible.

An uncertainty analysis has been carried out on the basis of the previous results. It has been verified that the proposed method is robust when used to estimate the injected quantity of the pilot pulses, as the average uncertainty is of the order of 0.15 mg. The average uncertainty in the prediction of the total injected quantity is of the order of 0.9 mg, and depends mainly on the accuracy of the evaluation of the heat transfer of the charge with the walls.

It has also been shown that the method is suitable for evaluating cycle-by-cycle variations of the injected quantities, provided that the input pressure is filtered. However, it has been verified that the use of the raw in-cylinder pressure allows the average injected quantities to be

849 estimated.

850 Finally, the approach is characterized by a very low computational time, that is, of the

851 order of 0.3 ms, when the elaboration is run on a PC and a crank angle integration step of 2 deg is

852 used, and is therefore suitable for control-oriented applications.

853

854 **ACKNOWLEDGMENTS**

856

857 **REFERENCES**

858 [1] Vanegas A, Won H, Felsch C, Gauding M. et al. Experimental Investigation of the Effect of

859 Multiple Injections on Pollutant Formation in a Common-Rail DI Diesel Engine. SAE Technical

860 Paper 2008-01-1191, 2008, doi:10.4271/2008-01-1191.

861 [2] Thurnheer T, Edenhauser D, Soltic P, Schreiber D, Kirchen P, Sankowski A. Experimental

862 investigation on different injection strategies in a heavy-duty diesel engine: Emissions and loss

863 analysis. Energ Convers Manage 2011; 52(1):457-467. doi: 10.1016/j.enconman.2010.06.074

864 [3] Catania AE, d'Ambrosio S, Ferrari A, Finesso R, Spessa E, Avolio G, Rampino V.

865 Experimental Analysis of Combustion Processes and Emissions in a 2.0L Multi-Cylinder Diesel

866 Engine Featuring a New Generation Piezo-Driven Injector. SAE Technical Paper 2009-24-0040,

867 2009, doi: 10.4271/2009-24-0040.

868 [4] Catania AE, Ferrari A., Manno M, Spessa E. Experimental Investigation of Dynamics

869 Effects on Multiple-Injection Common Rail System Performance. J. Eng. Gas Turbines Power

870 2008; 130(3): 032806-1-032806-13. doi: 10.1115/1.2835353.

871 [5] Catania AE, Ferrari A., Spessa E. Numerical-Experimental Study and Solutions to Reduce

872 the Dwell-Time Threshold for Fusion-Free Consecutive Injections in a Multijet Solenoid-Type CR

873 System. J Eng Gas Turbine Power 2008; 131(2): 022804-1-022804-14. doi: 10.1115/1.2938394.

874   [6] D'Ambrosio S, Ferrari A. Diesel Injector Coking: Optical-Chemical Analysis of

875   Deposits and Influence on Injected Flow-rate, Fuel Spray and Engine Performance. J Eng Gas

876   Turbine Power 2012; 134(6): 062801-1-062801-14. doi: 10.1115/1.4005991.

877   [7] Papagiannakis RG, Hountalas DT, Rakopoulos CD. Theoretical study of the effects of

878   pilot fuel quantity and its injection timing on the performance and emissions of a dual fuel

879   diesel   engine.   Energ   Convers   Manage   2007;   48(11):2951-2961.   doi:

880   10.1016/j.enconman.2007.07.003

881   [8] Finesso R, Misul DA, Spessa E. Development and Validation of a Semiempirical

882   Model for the Estimation of Particulate Matter in Diesel Engines. Energ Convers Manage

883   2014; 84:374-389. doi: 10.1016/j.enconman.2014.04.053.

884   [9] Ponti F, Corti E, Serra G, De Cesare M. Common Rail Multi-Jet Diesel Engine

885   Combustion Model Development for Control Purposes. SAE Technical Paper 2007-01-0383,

886   2007. doi:10.4271/2007-01-0383.

887   [10] Ponti F, Ravaglioli V, Moro D, Serra G. MFB50 On-Board Evaluation Based on a

888   Zero-Dimensional   ROHR   Model.   SAE   Technical   Paper   2011-01-1420,   2011.

889   doi:10.4271/2011-01-1420.

890   [11] Chmela FG, Orthaber GC. Rate of Heat Release Prediction for Direct Injection Diesel

891   Engines Based on Purely Mixing Controlled Combustion. SAE Technical Paper 1999-01-0186,

892   1999. doi:10.4271/1999-01-0186.

893   [12] Egnell R. A Simple Approach to Studying the Relation between Fuel Rate, Heat

894   Release Rate and NO Formation in Diesel Engines. SAE Technical Paper 1999-01-3548, 1999.

895   doi:10.4271/1999-01-3548.

896   [13] Catania AE, Finesso R, Spessa E. Predictive Zero-Dimensional Combustion Model for

897   DI Diesel Engine Feed-Forward Control. Energ Convers Manage 2011; 52(10):3159–3175, doi:

898   10.1016/j.enconman.2011.05.003.

899 [14] Catania AE, Finesso R, Spessa E, Catanese A, Landsmann G. Combustion Prediction by a

900 Low-Throughput Model in Modern Diesel Engines. SAE Int J Engines 2011; 4(1): 2106-2123. doi:

901 10.4271/2011-01-1410.

902 [15] Catania AE, Finesso R, Spessa E. Assessment of a Low-Throughput Predictive Model for

903 Indicated Cycle, Combustion Noise and NOx Calculation in Diesel Engines in Steady-State and

904 Transient Operations. ICES2012-81094, Proceedings of the ASME 2012 Internal Combustion

905 Engine Division Spring Technical Conference, May 6-9, 2012, Torino, Italy. doi:

906 10.1115/ICES2012-81094.

907 [16] Arcidiacono M, Baratta M, Finesso R, Kheshtinejad H, Misul D, Spessa E, Yang Y. Use of

908 an Innovative Predictive Heat Release Model Combined to a 1D Fluid-Dynamic Model for the

909 Simulation of a Heavy Duty Diesel Engine. SAE Int. J. Engines 2013; 6(3):1566-1579.

910 doi:10.4271/2013-24-0012.

911 [17] Alfieri V, Conte G, Finesso R, Spessa E, Yang Y. HRR and MFB50 Estimation in a Euro 6

912 Diesel Engine by means of Control-Oriented Predictive Models. SAE Int. J. Engines

913 8(3):1055-1068, 2015, doi:10.4271/2015-01-0879.

914 [18] Guido C, Beatrice C, Di Iorio S., Napolitano P et al. Assessment of Closed-Loop

915 Combustion Control Capability for Biodiesel Blending Detection and Combustion Impact

916 Mitigation for an Euro5 Automotive Diesel Engine. SAE Technical Paper 2011-01-1193, 2011,

917 doi:10.4271/2011-01-1193.

918 [19] Schmid U, Seidel H. Study on an injection quantity sensor. I: Evaluation of the integration

919 procedure. Journal of Micromechatronics 2005; 3(1):15 – 32. doi: 10.1163/156856305323383892.

920 [20] Schmid U, Seidel H. Study on an injection quantity sensor. II: Evaluation of the sensing

921 element. Journal of Micromechatronics 2005; 3(1):33 – 50. doi: 10.1163/156856305323383900.

922 [21] Finesso R, Spessa E. Ignition delay prediction of multiple injections in diesel engines. Fuel

923 2014; 119(1):170-190. doi: 10.1016/j.fuel.2013.11.040.

924   [22] D'Ambrosio S, Finesso R, Spessa E. Calculation Of Mass Emissions, Oxygen Mass

925   Fraction And Thermal Capacity Of The Inducted Charge In SI And Diesel Engines From Exhaust

926   And   Intake   Gas   Analysis.   Fuel   2011;   90(1):152–166,   doi:

927   http://dx.doi.org/10.1016/j.fuel.2010.08.025.

928   [23] Catania AE, Finesso R, Spessa E. Real-Time Calculation of EGR Rate and Intake

929   Charge Oxygen Concentration for Misfire Detection in Diesel Engines. SAE Technical Paper

930   2011-24-0149, 2011. doi: 10.4271/2011-24-0149.

931   [24] Heywood JB. Internal Combustion Engine Fundamentals. McGraw-Hill, New York,

932   1988.

933   [25] Finesso R, Spessa E. A Real Time Zero-Dimensional Diagnostic Model for the

934   Calculation of In-Cylinder Temperatures, HRR and Nitrogen Oxides in Diesel Engines. Energ

935   Convers Manage 2014; 79:498-510. doi: 10.1016/j.enconman.2013.12.045.

936   [26] Woschni G. A Universally Applicable Equation for the Instantaneous Heat Transfer

937   Coefficient in the Internal Combustion Engine. SAE Technical Paper 670931, 1967, doi:

938   10.4271/670931.

939   [27] Baratta M, d'Ambrosio S, Spessa E, Vassallo A. Cycle-Resolved Detection of

940   Combustion Start in SI Engines by Means of Different In-Cylinder Pressure Data Reduction

941   Techniques. ASME 2006 Internal Combustion Engine Division Spring Technical Conference

942   (ICES2006), doi: 10.1115/ICES2006-1367.

943   [28] ISO/IEC GUIDE 98-3:2008(E).

944   [29] Rocco V. Dynamic T.D.C. and Thermodynamic Loss Angle Measurement in a D. I.

945   Diesel Engine. SAE Technical Paper 851546, 1985, doi:10.4271/851546